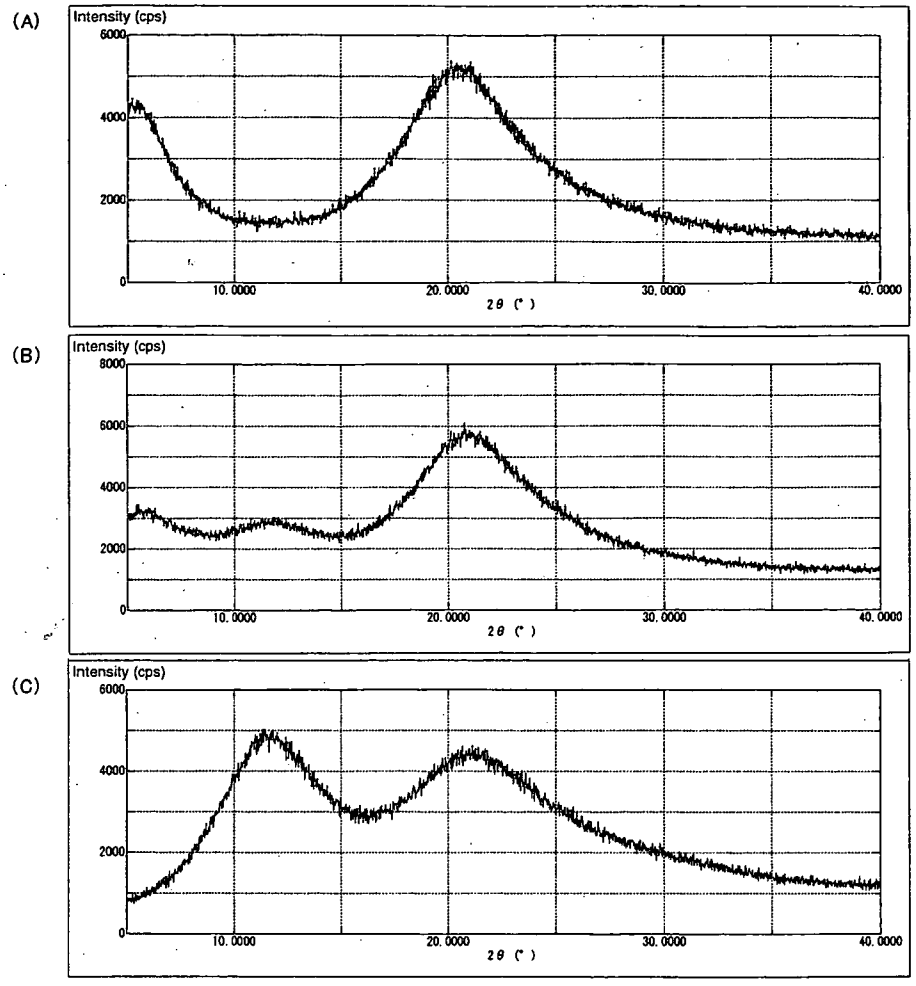

Fig. 2. Powder X-Ray Diffraction Patterns of PHPA (A), Nifedipine–PHPA (3 : 7) (B) and Nifedipine–PVP Solid Dispersions (3 : 7) (C)

mixture, the solid dispersion (3 : 7) showed mono-exponential T_1 decay, whereas bi-exponential $T_{1\rho}$ decay. These results indicate that nifedipine and PHPA are immiscible and that domains 5 to 50 nm in size are present in the solid dispersion. The nifedipine–PHPA solid dispersions (4 : 6 and 5 : 5) and the phenobarbital–PHPA solid dispersions (3 : 7) also exhibited bi-exponential $T_{1\rho}$ decay (data not shown). Figure 2 shows powder X-ray diffraction patterns of the nifedipine–PHPA and nifedipine–PVP solid dispersions. The observed halo pattern indicates that nifedipine in the PHPA dispersions is amorphous at the detection limit of powder X-ray diffractometry.

DSC data supported the contention that nifedipine and PHPA are immiscible. Figure 3 shows typical DSC traces for nifedipine–PHPA solid dispersions. The nifedipine–PHPA solid dispersion (3 : 7) showed glass transition at approximately 50 °C, corresponding to the T_g of amorphous nifedipine, and at approximately 75 °C, indicating that there are both an amorphous nifedipine phase and an amorphous nifedipine–PHPA phase in the solid dispersion. These DSC data indicate that amorphous nifedipine and PHPA are partially immiscible at this weight ratio. For the nifedipine–PHPA solid dispersion (5 : 5), T_g of the amorphous nifedipine–PHPA phase was not clearly observed because of the detection limit of DSC, suggesting that ^{1}H-NMR relaxation measurements can detect immiscibility of drugs and polymers more sensitively than DSC. DSC data suggest that the nifedipine–PHPA solid dispersion (3 : 7) consists of pure amorphous nifedipine phase and amorphous nifedipine–PHPA phase. NMR data may support this speculation. As shown in Fig. 1B, initial $T_{1\rho}$ decay of the solid dispersion was slower than that of the physical mixture or pure PHPA. This slow relaxation rate of the solid dispersion may indicate that the relaxation rate of PHPA protons was decreased by spin diffusion with nifedipine protons existing near PHPA molecules; in other words, nifedipine–PHPA phase is considered to exist in the solid dispersion. The effect of weight ratios on the $T_{1\rho}$ decay of nifedipine–PHPA solid dispersions needs to examine in order

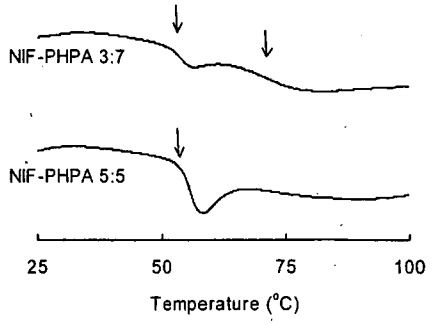

Fig. 3. DSC Traces for Nifedipine–PHPA Solid Dispersions
Arrows represent T_g.

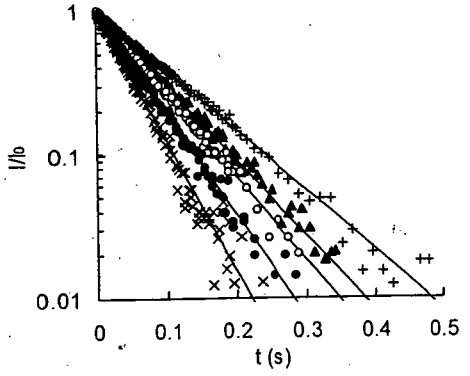

Fig. 4. $T_{1\rho}$ Decay Patterns for Nifedipine (+), PVP (×), and Nifedipine–PVP Solid Dispersions of 7 : 3 (▲), 5 : 5 (○), and 3 : 7 (●)

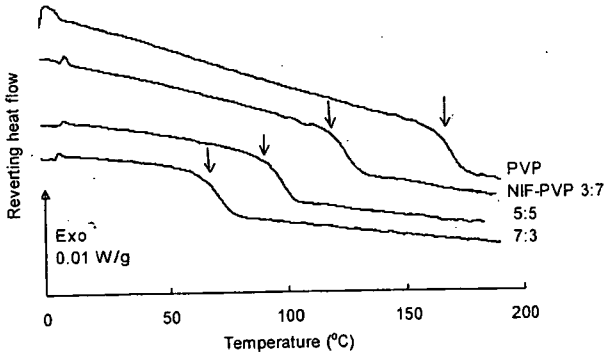

Fig. 5. DSC Traces for Nifedipine–PVP Solid Dispersions
Arrows represent T_g.

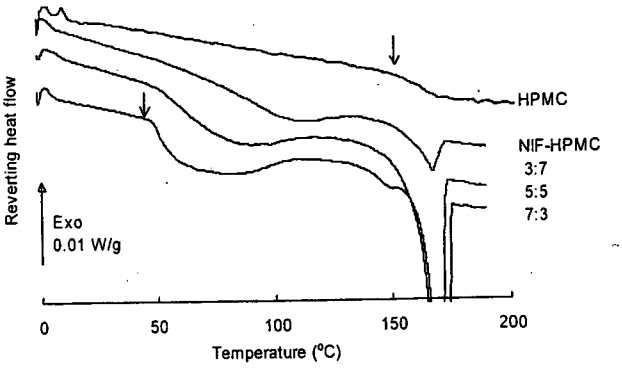

Fig. 6. DSC Traces for Nifedipine–HPMC Solid Dispersions
Arrows represent T_g.

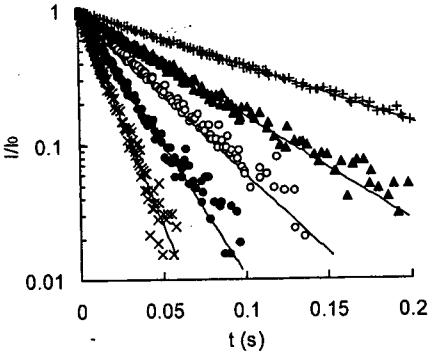

Fig. 7. $T_{1\rho}$ Decay Patterns for Nifedipine (+), HPMC (×), and Nifedipine–HPMC Solid Dispersions of 7 : 3 (▲), 5 : 5 (○), and 3 : 7 (●)

to confirm the phase structure of the solid dispersion, since the molecular mobility of PHPA may different from that of pure PHPA.

In contrast to PHPA, PVP and nifedipine in the solid dispersions (3 : 7, 5 : 5 and 7 : 3) were considered to be miscible from $T_{1\rho}$ relaxation and DSC measurements. Figure 4 shows typical $T_{1\rho}$ decay of the solid dispersions. All the solid dispersions studied exhibited mono-exponential $T_{1\rho}$ decay, whereas physical mixtures of amorphous nifedipine and PVP (3 : 7, 5 : 5 and 7 : 3) exhibited bi-exponential decay (data not shown). Figure 5 shows DSC traces for the nifedipine–PVP solid dispersions. A single glass transition was observed for all of the solid dispersions studied. These data indicate that nifedipine and PVP are miscible at the detection limit of NMR and DSC.

For nifedipine–HPMC solid dispersions, the miscibility of nifedipine and HPMC could not be assessed from T_g measurements. As shown in Fig. 6, base line shift due to glass transition was not obvious for the nifedipine–HPMC solid dispersions (3 : 7 and 5 : 5). In contrast to DSC measurements, $T_{1\rho}$ relaxation measurements clearly indicated that nifedipine is miscible with HPMC in the solid dispersions. As shown in Fig. 7, all the nifedipine–HPMC solid dispersions studied showed mono-exponential $T_{1\rho}$ decay. In contrast to the solid dispersions, physical mixtures of amorphous nifedipine and HPMC (3 : 7, 5 : 5 and 7 : 3) exhibited bi-exponential decay (data not shown). These data indicate that NMR can detect miscibility of a drug and an excipient more sensitively than DSC.

Figure 8 shows the dissolution profile of nifedipine from

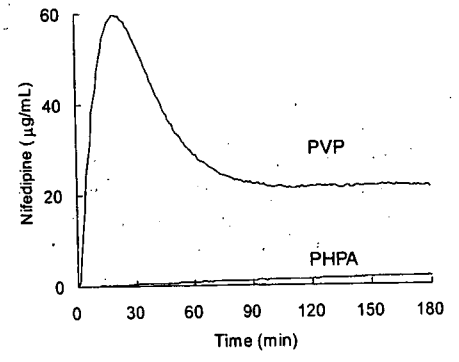

Fig. 8. Dissolution Profiles of Nifedipine from Solid Dispersions with PVP and PHPA

solid dispersions with PVP and PHPA. The nifedipine–PVP solid dispersion exhibited rapid dissolition of nifedipine with super-saturation. In contrast, only a minimal amount of nifedipine was dissolved from the nifedipine–PHPA solid dispersion.

In conclusion, ^{1}H- NMR spin–lattice relaxation measurements were found to be useful for assessing the miscibility of a drug and excipients in solid dispersions, especially, when T_g is not clearly detected by DSC. The lower miscibility of PHPA than that of PVP and HPMC with hydrophobic drugs is considered due to the more hydrophilic nature of PHPA.

Acknowledgements A part of this work was supported by a Grant-in-aid for Research on Publicly Essential Drugs and Medical Devices from The Japan Health Sciences Foundation.

References

1) Forster A., Hempenstall J., Tucker I., Rades T., *Int. J. Pharm.*, **226**, 147—161 (2001).
2) Lu Q., Zografi G., *Pharm. Res.*, **15**, 1202—1206 (1998).
3) Khougaz K., Clas S. D., *J. Pharm. Sci.*, **89**, 1325—1334 (2000).
4) Tong P., Zografi G., *J. Pharm. Sci.*, **90**, 1991—2004 (2001).
5) Vasanthavada M., Tong W. Q., Joshi Y., Kislalioglu M. S., *Pharm. Res.*, **21**, 1598—1606 (2004).
6) Shmeis R. A., Wang Z., Krill S. L., *Pharm. Res.*, **21**, 2025—2030 (2004).
7) Kaplan D. S., *J. Appl. Polym. Sci.*, **20**, 2615—2629 (1976).
8) Crowly K. J., Zografi G., *J. Pharm. Sci.*, **91**, 2150—2165 (2002).
9) Marsac P. J., Shamblin S. L., Taylor L. S., *Pharm. Res.*, **23**, 2417—2426 (2006).
10) Cheung M. K., *Polymer*, **41**, 1469—1474 (2000).
11) Asano A., Takegoshi K., "Solid State NMR of Polymers," Chap. 10, ed. by Ando I., Asakura T., Elsevier, Amsterdam, 1998, pp. 351—414.
12) Giammona G., Carlisi B., Plazzo S., *J. Polym. Sci. Polym. Chem. Ed.*, **25**, 2813—2818 (1987).
13) Kato Y., Watanabe F., *Yakugaku Zasshi*, **98**, 639—648 (1978).
14) Aso Y., Yoshioka S., Kojima S., *J. Pharm. Sci.*, **89**, 408—416 (2000).

Journal of
Nanoscience and Nanotechnology
Vol. 8, 1–6, 2007

Polymeric Micelles Modified by Folate-PEG-Lipid for Targeted Drug Delivery to Cancer Cells *In Vitro*

Akihiro Hayama[1], Tatsuhiro Yamamoto[2], Masayuki Yokoyama[2], Kumi Kawano[1], Yoshiyuki Hattori[1], and Yoshie Maitani[1,*]

[1] *Institute of Medicinal Chemistry, Hoshi University, 2-4-41 Ebara, Shinagawa-ku, Tokyo 142-8501, Japan*
[2] *Kanagawa Academy of Science and Technology, KSP East 404, Sakado 3-2-1, Takatsu-ku, Kawasaki-shi, Kanagawa 213-0012, Japan*

A novel technique was developed for the formation of ligand-targeted polymeric micelles that can be applicable to various ligands. For tumor-specific drug delivery, camptothecin (CPT)-loaded polymeric micelles were modified by folate to produce a folate-receptor-targeted drug carrier. Folate-linked PEG_{5000}-distearoylphosphatidylethanolamine (folate-PEG_{5000}-DSPE) was added when preparations of drug-loaded polymeric micelles, resulting in folate ligands exposed to the surface. Folate-modified CPT-loaded polymeric micelles (F-micelle) were evaluated by measuring cellular uptake using a flow cytometer, fluorescence microscopy, and confocal laser scanning microscopy, and by cytotoxicity measurement. The results revealed that F-micelle showed higher cellular uptake in KB cells over-expressing folate receptor (FR) and higher cytotoxicity compared with non-folate modified CPT-loaded polymeric micelles (plain micelles) in KB cells, but not in FR-negative HepG2 cells. This result indicated that polymeric micelles were successfully modified by the folate-linked lipid.

Keywords: Polymeric Micelles, Camptothecin, Targeting, Folate-PEG-Lipid, Folate.

RESEARCH ARTICLE

1. INTRODUCTION

Camptothecin (CPT) has shown a broad spectrum of antitumor activity;[1,2] however, its clinical use of CPT has some drawbacks, mainly due to water insolubility and aqueous instability of the lactone ring moiety. The lactone ring opens rapidly at physiological pH or above, resulting in a complete loss of biological activity.[3,4]

Nanoparticles including polymeric micelles have attracted much attention in drug delivery research. Polymeric micelles are prepared from block copolymers possessing both hydrophilic and hydrophobic chains.[5,6] Their advantageous characteristics for drug targeting include solubilization of hydrophobic molecules and high structural stability. CPT-loaded polymeric micelles enhanced the anticancer activity of CPT against solid tumors because of their prolonged blood circulation and higher accumulation in tumors.[7,8]

As with other carriers, ligand-mediated targeting of polymeric micelles to target receptors expressed selectively or over-expressed on tumor cells is increasingly recognized as an effective strategy for improving the therapeutic effect of anticancer drugs. If CPT can facilitate tumor targeting, a great contribution to the cancer chemotherapy is feasible. A variety of targeting ligands has been examined as tumor-targeted drug carriers. Folate receptor (FR) is abundantly expressed in a large percentage of human tumors, but it is only minimally distributed in normal tissue;[9] therefore, FR can serve as a functional tumor-specific receptor. Folate modification of polymeric micelles has been reported to covalently conjugate block copolymer with folate.[10,11] In these methods, the type of ligand must be decided in the preparation of polymeric micelles. In other words, the ligand-polymer conjugate must be synthesized with conformity to the drug. It is already known that a proper amount of folate-PEG-lipids could be inserted in liposomes and emulsions without change of their stability, and folate lipid-modified liposomes and emulsions with longer polyethylene glycol (PEG) linker were taken effectively by the FR-mediated cellular uptake.[12,13] However, it has been no reports about surface-modified polymeric micelles by lipid. In polymer micelles, folate might not be able to be exposed outside by steric configuration of the hydrophilic block chain. Properties of the inner core such as hydrophobicity and rigidity, were very important to achieve micelles with stable drug incorporation.[7,8,14] Folate lipid modification, therefore might affect the properties of the inner cores.

*Author to whom correspondence should be addressed.

1533-4880/2007/8/001/006 doi:10.1166/jnn.2007.093

For targeted drug delivery to cancer cells, we prepared folate-modified CPT-loaded polymeric micelles (F-micelle), and evaluated by measuring cellular uptake using a flow cytometer, fluorescence microscopy, and confocal laser scanning microscopy, and by cytotoxicity measurement. In this paper, we describe a novel method of folate modification to CPT-loaded polymeric micelles by folate-linked PEG_{5000}-distearoylphosphatidylethanolamine (folate-PEG_{5000}-DSPE).

2. MATERIALS AND METHODS

2.1. Materials

Poly(ethylene glycol)-poly(benzyl aspartate-53) block copolymer (PEG-P(Asp(Bz53))) was synthesized as described previously.[14,15] The molecular weight of the PEG block was 2000 and the average number of aspartate units was 17. Fifty-three percentage of the aspartic acid residue was esterified with the benzyl group. CPT and folic acid were purchased from Wako Pure Chemicals (Tokyo, Japan). Folate-PEG_{5000}-DSPE was synthesized as described previously.[12,13] 1,1′-Dioctadecyl-3,3,3′,3′-tetramethylindocarbocyanine perchlorate (DiI) was purchased from Lambda Probes and Diagnostics (Graz, Austria).

2.2. Preparation of Folate-Modified CPT-Loaded Polymeric Micelles (F-Micelles)

CPT was incorporated into polymeric micelles by an evaporation method as described previously,[15] using 0.5 mg of CPT, 5 mg of block copolymer, and 0 mol%, 0.03 mol% (0.027 mg), 0.1 mol% (0.092 mg) and 0.2 mol% (0.18 mg) of folate-PEG_{5000}-DSPE to CPT loaded in micelles for plain micelles, 0.03F-micelle, 0.1F-micelle and 0.2F-micelle, respectively. DiI-labeled F-micelles were prepared by the same protocol, but with the post-addition of DiI at 0.4 mol% of incorporated CPT. The incorporation efficiency was calculated as described previously.[15] The mean particle diameters and ζ-potentials were determined using a particle size analyzer (ELS-Z, Otsuka Electronics, Osaka, Japan) at 25 °C by diluting the dispersion to an appropriate volume with water.

2.3. *In Vitro* Drug Release

Release of CPT in F-micelles from a dialysis tube was measured using seamless cellulose tube membranes (Viskase Sales Corp., IL, USA) with a molecular cut-off of 12,000–14,000. The initial concentration of CPT was 10 μg/ml. The sample volume in the dialysis bag was 1 ml and the sink volume was 200 ml PBS at pH 7.4 with the medium at 37 ± 0.1 °C. The drug concentration was analyzed using fluorescence spectrophotometer F-4010 (Hitachi, Tokyo, Japan) (excitation 369 nm, emission 426 nm).

2.4. Cell Culture

KB cells (FR (+)) and HepG2 cells (FR (−)) were obtained from the Cell Resource Center for Biomedical Research, Tohoku University (Miyagi, Japan). Both cells were cultured in folate-deficient RPMI 1640 medium (Invitrogen Corp., Carlsbad, CA, USA) with 10% heat-inactivated fetal bovine serum (Invitrogen Corp.) and 100 μg/ml kanamycin with 5% CO_2 at 37 ° C.

2.5. Flow Cytometry Analysis

KB cells were prepared by plating 5×10^5 cells in a 6-well culture plate 1 day before the assay. Cells were incubated with DiI-labeled F-micelles containing 10 μg CPT/ml diluted in 2 ml folate-deficient RPMI 1640 medium for 2 hours at 37 °C. In free-folic acid competition studies, 2 mM folic acid was added to the medium. After incubation, cells were washed two times with acidic saline (pH 3) followed by one wash with cold phosphate-buffered saline (PBS, pH 7.4) to remove unbound polymeric micelles, detached with 0.02% EDTA-PBS, and then suspended in PBS containing 0.1% bovine serum albumin and 1 mM EDTA. The suspended cells were directly introduced to a FACSCalibur flow cytometer (Becton Dickinson, San Jose, CA, USA) equipped with a 488 nm argon ion laser. Data for 10,000 fluorescent events were obtained by recording forward scatter, side scatter, and 585/42 nm fluorescence. The autofluorescence of cells was taken as a control.

2.6. Fluorescence and Confocal Laser Scanning Microscopy

After incubation, cells were washed as described above; 2 ml fresh medium was added. The cells were observed with fluorescence microscopy (ECLIPSE TS100, Nikon, Tokyo, Japan) at just. For confocal laser scanning microscopy, cells were fixed with Mildform 20 N for 30 min at room temperature. Subsequently, the cells were washed three times with PBS. Examinations were performed with a Radiance 2100 confocal laser-scanning microscope (BioRad, CA, USA).

2.7. Cytotoxicity Study

Cells were prepared by plating 1×10^4 cells in a 96-well culture plate 1 day before the experiment. KB and HepG2 cells were then incubated for 2 hours at 37 °C with 100 μl CPT solution, plain micelle, and F-micelles (containing 0.01, 0.1, 0.5, 1, 2.5 and 5 μg CPT) diluted in folate-deficient RPMI 1640 medium. The medium was replaced with fresh medium and incubated for a further 48 hours. Cytotoxicity was determined with the WST-8 assay (Dojindo Laboratories, Kumamoto, Japan). The number of viable cells was then determined by absorbance measured at 450 nm on an automated plate reader (BioRad, CA, USA).

RESEARCH ARTICLE

2.8. Statistical Analysis

Statistical comparisons were performed by Student's t-test. P values less than 0.05 were considered significant.

3. RESULTS AND DISCUSSION

3.1. Determination of CPT Content and Particle Size of F-Micelles

In our previous study, folate modification with a sufficiently long PEG chain on emulsion is an effective way of targeting drug carriers to tumor cells.[13] Therefore, folate-lipid conjugate with PEG_{5000} linker was used for the modification of polymeric micelles with PEG_{2000}. Four kinds of CPT-loaded polymeric micelles were formulated as plain micelles, 0.03F-micelle, 0.1F-micelle and 0.2F-micelle. Folate-PEG-DSPE may be incorporated to polymeric micelles since 0.2 mol% folate-PEG_{5000}-DSPE was 9.6 μM, and the critical micelle concentration (CMC) value of folate-PEG_{5000}-DSPE was 12.1 μM determined by the fluorescence probe technique using DiI.

The average particle size of each F-micelle in water was about 230 nm with 0.5–1.1 mV in ζ-potential and the CPT-loading efficiency was about 50%. These values of F-micelles did not change significantly compared with plain micelles.

3.2. *In Vitro* Drug Release

The *in vitro* release of CPT from 0.03F-micelle exhibited rapid release behavior in an early stage (about 40% in 2 hours, Fig. 1). In contrast, the release of CPT from 0.2F-micelle and plain micelles reached only about 20% after the same period of incubation. This result indicates that the quantity of folate modification affected the stability of polymeric micelles, indicating that the higher the folate surface density, the lower the drug release. Similar results were reported that folate modification of liposomes influenced the release pattern.[16] The decreased drug release from highly folate-modified polymer micelles might be due to the structural integrity of folate coupling, that may lead to barrier effect for CPT diffusion.

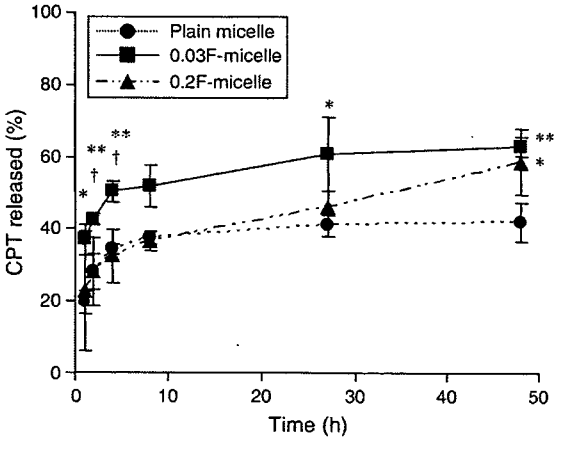

Fig. 1. Release profiles from plain and folate-modified CPT-loaded polymeric micelles at 37 °C in PBS as a sink solution at pH = 7.4. Each value represents the mean ± S.D. ($n = 3$). $^{*}P < 0.05$, $^{**}P < 0.01$ compared with plain micelle, $^{\dagger}P < 0.05$ compared with 0.2F-micelle.

3.3. Uptake of F-Micelles to KB Cells

Cellular uptake of F-micelle was evaluated using polymeric micelles labeled with DiI by flow cytometry. The fluorescence of 10 μg CPT/ml of DiI-labeled plain

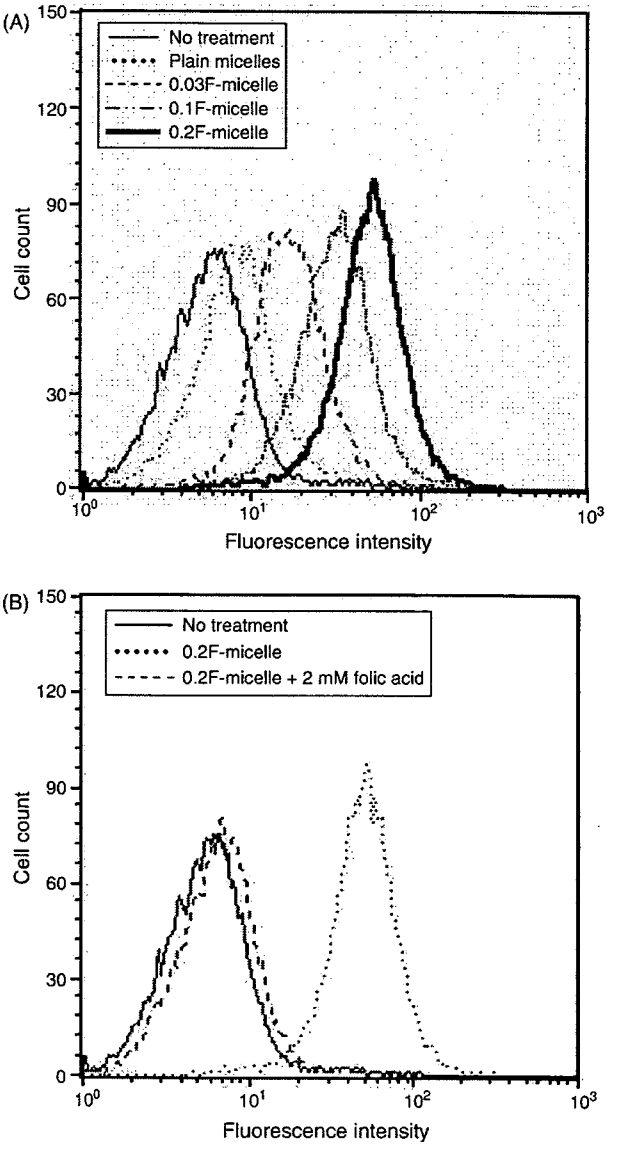

Fig. 2. Uptake of DiI-labeled plain and folate-modified CPT-loaded polymeric micelles with KB cells in the absence (A), or presence of 2 mM folic acid (B). Cells were incubated with polymeric micelles in folate-free RPMI 1640 medium for 2 hours at 37 °C and analyzed by flow cytometry. No treatment indicates autofluorescence of untreated cells. Each analysis was generated by counting 10^4 cells.

RESEARCH ARTICLE

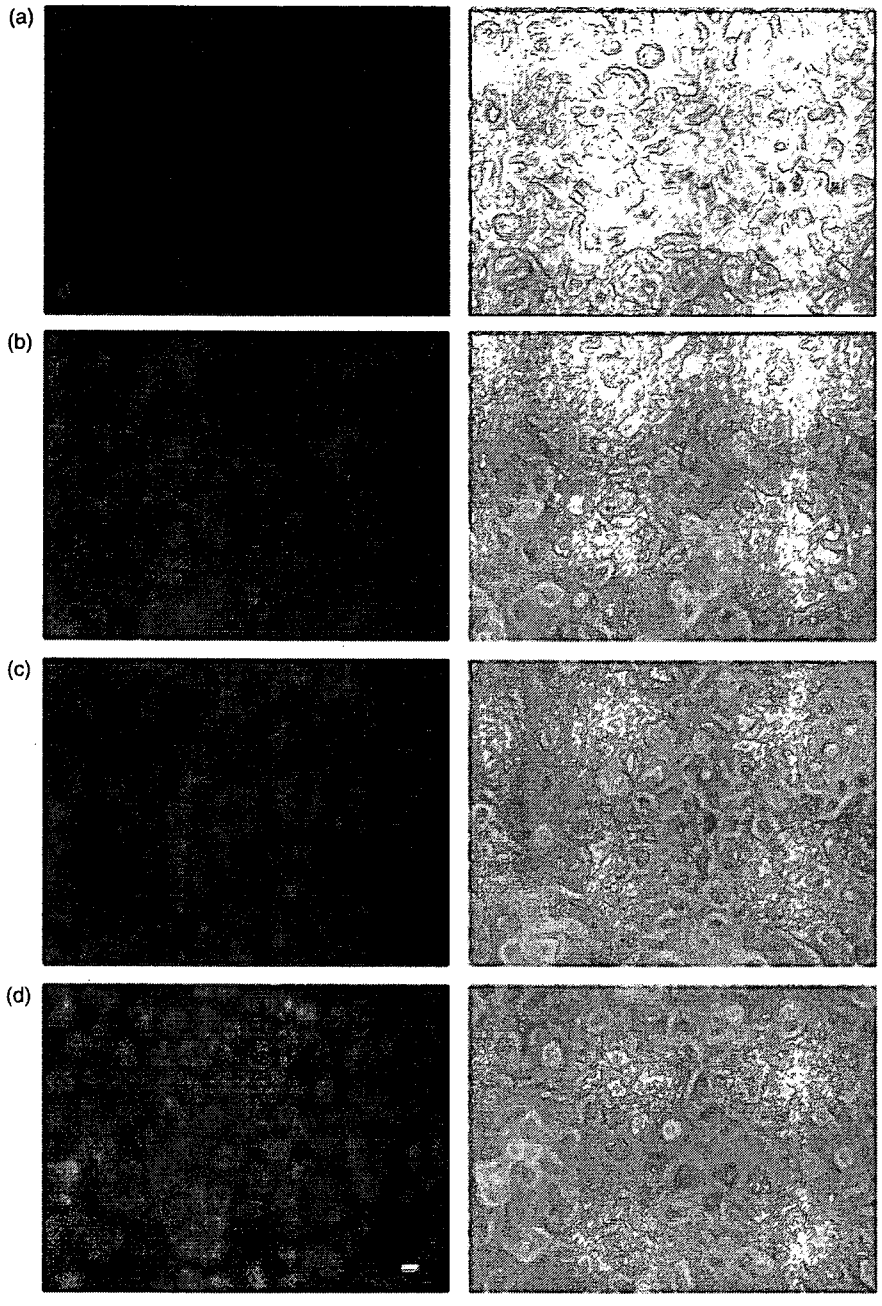

Fig. 3. Fluorescence microscopic images of KB cells treated with (a) plain micelles, (b) 0.03F-micelle, (c) 0.1F-micelle and (d) 0.2F-micelle. Cells were incubated with polymeric micelles in folate-free RPMI 1640 medium for 2 hours at 37 °C, then observed just after. (×200) Scale bar denotes 10 μm.

micelles and F-micelles showed almost identical spectrofluorimetric units (data not shown). As shown in Figure 2(A), flow cytometry analysis represented a shift in the curve. 0.2F-micelle indicated higher mean intensity of about 13.8-fold, 7.9-fold and 3.3-fold in cellular association of plain micelles, 0.03F-micelle and 0.1F-micelle after 2 hours exposure, respectively. In contrast, micelles modified with methoxy-PEG_{5000}-DSPE showed a similar curve to plain micelles (data not shown). Additionally, these increased associations of 0.03F-micelle, 0.1F-micelle (data not shown) and 0.2F-micelle could be completely blocked by adding 2 mM folic acid to the medium (Fig. 2(B)). This is the first report showing that folate-lipid was incorporated and its folate group was exposed on the surface of polymeric micelles to interact with FR. The results also indicate that F-micelle was transported within cells by an FR-mediated endocytosis process. These findings are consistent with those reported previously on the FR-mediated cellular uptake of folate-modified liposomes and emulsions for anti-cancer therapy.[12, 13]

Cellular uptake of F-micelles was also evaluated using fluorescence microscopy. Fluorescence images of KB cells after incubation with F-micelles for 2 hours are shown in Figure 3. For plain micelles, there was no remarkable uptake in fluorescent intensity of KB cells. In contrast, in F-micelles, more fluorescently labeled cells could be clearly visualized, and 0.2F-micelle was especially taken up in to the cells. This result is similar to that of flow cytometry. In accordance with the results from flow cytometry analysis, fluorescence microscopy confirmed that F-micelles could be targeted to cancer cells over-expressing FR on their surface.

3.4. Localization of F-Micelles to KB Cells

To investigate whether F-micelles existed on cell surface or within cells, localization of F-micelles was evaluated using confocal laser scanning microscopy. Fluorescence images of KB cells after incubation with 0.03F-micelle for 2 hours are shown in Figure 4. 0.2F-micelle showed similar image (data not shown). The localization of DiI-labeled F-micelles was confirmed by changing the Z-axis of observed area with 1 μm. DiI-fluorescence was detected as punctuate dots within cells. This indicated that F-micelles were internalized into the cells and located within endosome compartments.

3.5. Cytotoxicity Study

FR-targeted polymeric micelles were evaluated for *in vitro* cytotoxicity in FR (+) KB and FR (−) HepG2 cells by WST-8 assay. Superior cytotoxicity of F-micelles over plain micelles was observed in KB cells, but not in HepG2 cells. IC_{50} values for KB cells of F-micelles were about 2–3 times lower than the plain micelles (Table I). The difference of IC_{50} values between 0.03F-micelle and 0.2F-micelle was not large. It might be due to the release of CPT from 0.03F-micelle was faster than that from 0.2F-micelle, and free CPT was taken up to the cells as well as micelles. In contrast, IC_{50} values for HepG2 cells show hardly any difference between F-micelles and plain micelles.

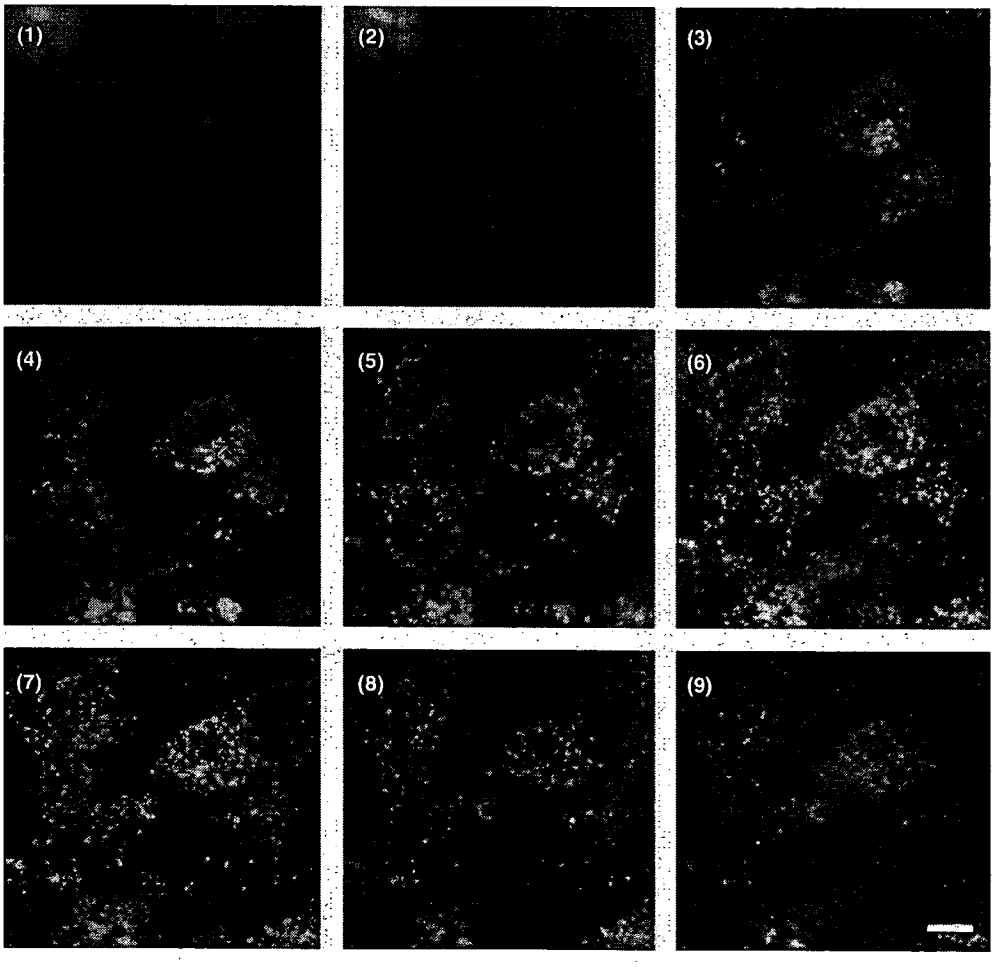

Fig. 4. Localization of DiI-labeled folate-modified CPT-loaded polymeric micelles (0.03F-micelle) with KB cells. Cells were incubated with polymeric micelles in folate-free RPMI 1640 medium for 2 hours at 37 °C, then observed just after under confocal laser scanning microscopy by changing the Z-axis. Images (1–9) represent regular intervals of 1 μm on the Z-axis from bottom to top cells, respectively. (×1200) Scale bars denote 10 μm.

Table I. IC_{50} value (μg/ml) of CPT solution, plain micelles, folate-modified CPT-loaded polymeric micelles for KB cells and HepG2 cells.

		Polymeric micelles			
Cells	CPT-solution	Plain	0.03F	0.1F	0.2F
KB	3.0±0.4	6.7±1.1	2.2±0.5	3.6±0.8	2.1±0.9
HepG2	2.2±0.2	8.7±0.9	8.4±0.4	7.4±1.0	6.5±1.6

Data are shown as the mean±S.D. ($n = 3$).

The CPT lactone ring opened at about 20 minutes in medium.[3] The lactone E-ring in CPT plays an important role in a drug's biological activity but it exists in a pH-dependent equilibrium in an open ring carboxylate form. Incorporation of CPT in micelles could maintain active lactone form even in the presence of serum,[14] indicating that micelle formulations could keep the antitumor effect of CPT. Plain micelles showed lower cytotoxicity than CPT solution, because the PEG shells of polymeric micelles inhibited interaction with cells. However, folate modification of polymeric micelles increased the association with cells via FR, resulting in increase of the cytotoxicity similar to CPT solution. It is one of the reasons that IC_{50} values of F-micelles were much higher or similar to those for CPT solution. Preferential partitioning of the lactone form into lipid layers has been previously reported to stabilize CPT.[3,17] *In vivo* situation, micelle formulation enhanced the accumulation in tumor tissue than CPT solution.[8] Further interaction of folate may increase the antitumor effect of CPT micelles. These results indicate that 0.2F-micelle is suitable drug carrier for selective drug delivery and is more adapted than 0.03F-micelle.

4. CONCLUSION

Uptake and cytotoxicity study showed that F-micelles could be selectively taken into cancer cells by folate-receptor mediated endocytosis. The novel lipid-based modification method to polymeric micelles is applicable to antibody, peptides, or other ligands. Furthermore, this allows double targeting using folate-lipid and another ligand-conjugated polymeric micelles or folate-targeted therapeutics to be tailored to the needs of individual patients.

Acknowledgments: This work was supported by Grants-in-Aids from the Ministry of Health, Labour and Welfare of Japan. We are grateful to Mr. Atsushi Yamada and Mr. Takashi Yoshizawa for providing folate-PEG_{5000}-DSPE.

References and Notes

1. B. C. Giovanella, H. R. Hinz, A. J. Kozielski, J. S. Stehlin, Jr., R. Silber, and M. Potmesil, *Cancer Res.* 51, 3052 (**1991**).
2. B. C. Giovanella, J. S. Stehlin, M. E. Wall, M. C. Wani, A. W. Nicholas, L. F. Liu, R. Silber, and M. Potmesil, *Science* 246, 1046 (**1989**).
3. T. G. Burke, A. E. Staubus, and A. K. Mishra, *J. Am. Chem. Soc.* 114, 8318 (**1992**).
4. J. Fassberg and V. J. Stella, *J. Pharm. Sci.* 81, 676 (**1992**).
5. K. Kataoka, A. Harada, and Y. Nagasaki, *Adv. Drug Deliv. Rev.* 47, 113 (**2001**).
6. V. P. Torchilin, *Mol. Life Sci.* 61, 2549 (**2004**).
7. M. Watanabe, K. Kawanos, M. Yokoyama, P. Opanasopit, T. Okano, and Y. Maitani, *Int. J. Pharm.* 308, 183 (**2006**).
8. K. Kawano, M. Watanabe, T. Yamamoto, M. Yokoyama, P. Opanasopit, T. Okano, and Y. Maitani, *J. Control. Release* 112, 329 (**2006**).
9. M. Wu, M. Gunning, and M. Ratnam, *Biomarkers Prev.* 8, 775 (**1999**).
10. P. V. Paranjpe, Y. Chen, V. Kholodovych, W. Welsh, S. Stein, and P. J. Sinko, *J. Control. Release* 100, 275 (**2004**).
11. H. S. Yoo and T. G. Park, *J. Control. Release* 96, 273 (**2004**).
12. A. Gabizon, A. T. Horowitz, D. Goren, D. Tzemach, F. Mandelbaum-Shavit, M. M. Qazen, and S. Zalipsky, *Bioconjug. Chem.* 10, 289 (**1999**).
13. T. Shiokawa, Y. Hattori, K. Kawano, Y. Ohguchi, H. Kawakami, K. Toma, and Y. Maitani, *Clin. Cancer Res.* 11, 2018 (**2005**).
14. P. Opanasopit, M. Yokoyama, M. Watanabe, K. Kawano, Y. Maitani, and T. Okano, *Pharm. Res.* 21, 2001 (**2004**).
15. M. Yokoyama, P. Opanasopit, T. Okano, K. Kawano, and Y. Maitani, *J. Drug Target.* 12, 373 (**2004**).
16. Y. Gupta, A. Jain, P. Jain, and S. Jain, *J. Drug Target.* 15, 231 (**2007**).
17. Y. Sadzuka, S. Hirotsu, and S. Hirota, *Jpn. J. Cancer Res.* 90, 226 (**1999**).

Received: 20 June 2007. Accepted: 8 August 2007.

RESEARCH ARTICLE

Journal of
Nanoscience and Nanotechnology
Vol. 8, 1–8, 2008

Decaarginine-PEG-Artificial Lipid/DNA Complex for Gene Delivery: Nanostructure and Transfection Efficiency

Masahiko Furuhata[1], Radostin Danev[2], Kuniaki Nagayama[2], Yoshifumi Yamada[3], Hiroko Kawakami[4], Kazunori Toma[4], Yoshiyuki Hattori[1], and Yoshie Maitani[1,*]

[1] *Institute of Medicinal Chemistry, Hoshi University, Shinagawa-ku, Tokyo 142-8501, Japan*
[2] *National Institutes of Natural Sciences, Okazaki-shi, Aichi 444-8787, Japan*
[3] *Life Science Group, Olympus Corporation, Hachioji-shi, Tokyo 192-8512, Japan*
[4] *The Noguchi Institute, Itabashi-ku, Tokyo 173-0003, Japan*

Oligoarginine conjugates are highly efficient vectors for the delivery of plasmid DNA into cells. Decaarginine-conjugated lipid (Arg10-PEG-lipid) was synthesized and the effects of Arg10-PEG-lipid concentration at a fixed DNA concentration on transfection efficiency and the structure of the complexes were studied below and above critical micelle concentration (CMC), and at the lipid nitrogen/DNA phosphate (N/P) ratio corresponding to transfection, respectively. Arg10-PEG-lipid at the concentration below CMC showed stronger interaction with DNA by fluorescence intensity distribution analysis, and significantly higher luciferase and green fluorescent protein expression than that above CMC. A phase-contrast cryo-transmission electron microscope (cryo-TEM) experiment showed that the morphology of the complexes depended on the N/P ratio. At a low N/P ratio corresponding to that in transfection at a lipid concentration below CMC, a net-like structure developed in which plasmid DNA was involved. A further increase in the N/P ratio, a large fibrous nanostructure of complexes, was also observed. Without DNA, these structures were not obtained. The cellular uptake mechanism of complexes using flow cytometry with inhibitors suggested that complexes with two different morphologies showed similar cellular uptake and uptake mechanism, macropinocytosis. Differences in transfection efficiency of the complexes may be explained by a large fibrous nanostructure inhibiting the cellular internalization of complexes or the release of DNA from macropinosomes into cytoplasm. Arg10-PEG-lipid/DNA complexes formed a favorable nanostructure for gene delivery, depending on the N/P ratio in water.

Keywords: Decaarginine, Cell-Penetrating Peptide, Macropinocyotosis, Gene Delivery, Supramolecular Structure.

RESEARCH ARTICLE

1. INTRODUCTION

The development of a gene delivery vector is believed to be a key to the success of gene therapy. Gene delivery vectors are classified into viral and nonviral vectors. Viral vectors provide very high transfection efficiency, but their safety is a great concern because of their immunogenicity and acute toxicity.[1,2] For the future development of gene therapy, a safe and highly effective nonviral gene vector is indispensable, and nonviral vectors such as cationic liposomes and polymers have been developed;[1,3,4] however, their low-level transfection efficiency, compared with viral vectors, is considered to be a major limitation in their application to gene therapy. Poor efficiency is supposed to arise from the endocytic route of internalization, when cationic lipids or polymers form a complex with DNA; therefore, novel and more efficient synthetic vectors, hopefully with a different cell internalization mechanism, are desired.

Oligoarginine is known as a cell-penetrating peptide (CPP),[5–7] and can deliver its associated molecules into cells.[8–11] In our previous work, we reported oligoarginine ((Arg)n; $n = 4, 6, 8, 10$)-conjugated lipids with a poly(ethylene glycol) (PEG) spacer as novel gene vectors.[12] (Arg)n-PEG-lipid provides three characteristic functions: the PEG-lipid part forms micelles, the (Arg)n part can interact with DNA and make it compact, and this part

*Author to whom correspondence should be addressed.

1533-4880/2008/8/001/008 doi:10.1166/jnn.2008.170

also interacts with cells as CPP. Arg10-PEG-lipid showed the highest transfection efficiency among (Arg)*n*-PEG-lipids in human cervical carcinoma HeLa cells when the lipid formed a complex with plasmid DNA at concentrations much higher than their critical micelle concentration (CMC) to ensure the integrity of micelles.[12] Transfection efficiency was comparable to Lipofectamine 2000, a commercial transfection reagent.[12]

Cationic lipids form small particles when they form a complex with DNA molecules, which is an ideal property for efficient internalization of the complexes by endocytosis.[13] A variety of structural models have been proposed based upon electron microscopy studies about cationic liposome complexes with DNA by using a nature of helper lipids. The superior transfection properties of lipoplexes were related to its ability to undergo a lamellar to a nonlamellar phase.[14] About micelles, however, information of morphologies of complexes depending charge ratios of lipid/DNA was poor.[15] Below CMC, the relationship between transfection efficiency and structure of lipid complexes with DNA were not reported to our knowledge.

The purpose of this study was to investigate the relationship of the concentration of Arg10-PEG-lipid to lipid-mediated gene delivery. The interaction between Arg10-PEG-lipid and plasmid DNA was measured by fluorescence intensity distribution analysis (FIDA), and the morphology of Arg10-PEG-lipid/DNA complex was observed by phase contrast cryo-transmission electron microscopy (phase contrast cryo-TEM). Here, we report novel aspects of Arg10-PEG-lipid, i.e., the concentration-dependent transfection efficiency and relationship with nanostructure formation that may cause difference in the ability to deliver DNA into HeLa cells. The lipid showed higher transfection at a concentration below CMC than above CMC.

RESEARCH ARTICLE

2. MATERIALS AND METHODS

2.1. Materials

The Pica gene luciferase assay kit was purchased from Toyo Ink (Tokyo, Japan). Bicinchonic acid (BCA) protein assay reagent was obtained from Pierce (Rockford, IL). Dulbecco's modified Eagle's medium (DMEM) and fetal bovine serum (FBS) were purchased from Invitrogen Corp. (Carlsbad, CA). 5-(*N*-ethyl-*N*-isopropyl) amiloride (EIPA) was from Sigma Chemical Co. (St. Louis, MO). All other chemicals used were of reagent grade.

Arg10-PEG-lipid (Arg10-PEG-BDB, Fig. 1) and 7-nitrobenz-2-oxa-1,3-diazole (NBD)-labeled Arg10-PEG-BDB (Arg10-PEG-BDB-NBD) were synthesized as described previously.[12] 3,5-Bis(dodecyloxy)benzamide (BDB) was employed as the lipid component, and a PEG (MW = 2 kDa) spacer was introduced between the C-terminal of Arg10 and the amide group of BDB.

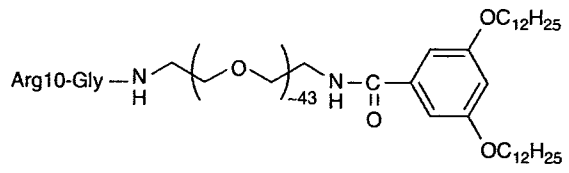

Fig. 1. Chemical structure of Arg10-PEG-BDB.

The plasmid DNA encoding the luciferase gene under the control of the CMV promoter (pCMV-luc) was constructed as previously described.[16] The plasmid pEGFP-C1 encoding the green fluorescent protein (GFP) under the CMV promoter was purchased from Clontech (Palo Alto, CA). A protein-free preparation of pCMV-luc and pEGFP-C1 was purified following alkaline lysis using maxiprep columns (Qiagen, Hilden, Germany). Labeling of pCMV-luc was performed using the protocol of a Label IT TM-rhodamine labeling kit (Mirus, Madison, WI).

2.2. Critical Micelle Concentration of Arg10-PEG-BDB

In order to determine the critical micelle concentration (CMC) of Arg10-PEG-BDB, fluorescence measurements were carried out using pyrene (0.6 μM) as reported in the literature.[17] The fluorescence emission spectra of pyrene were measured at varying Arg10-PEG-BDB concentrations using a fluorescence spectrometer. The concentration of Arg10-PEG-BDB used was within the range from 1×10^{-8} to 1×10^{-3} M. Pyrene was dissolved in acetone and transferred into capped tubes. The acetone as solvent was evaporated off by a stream of dry nitrogen, and subsequently, aqueous solutions of Arg10-PEG-BDB micelles were added. Then, the micellar solutions containing pyrene were heated to 80 °C for 2 h to equilibrate the partitioning of pyrene into the micelles and were allowed to cool over night at room temperature in the dark.

2.3. Formulation of Arg10-PEG-BDB/DNA Complex

Arg10-PEG-BDB stock solutions (20 mg/mL) were prepared by dissolving lipid in MilliQ water. Arg10-PEG-BDB/DNA complexes were formulated by mixing DNA and Arg10-PEG-BDB stock solutions. The number of nitrogen of Arg10-PEG-BDB was defined as 10 and the lipid nitrogen/DNA phosphate (N/P) ratio was calculated. For transfection and FIDA experiments, the following amounts of the Arg10-PEG-BDB to 2 μg of DNA were used to prepare Arg10-PEG-BDB/DNA complexes at various N/P ratios, e.g., N/P = 8.5; 20 μg/mL (5 μM). For transmission electron microscopy experiment, 0.25 mM of Arg10-PEG-BDB/DNA (N/P = 8.5/1) and 1.25 mM of Arg10-PEG-BDB/DNA (N/P = 42.5/1) were used, since higher Arg10-PEG-BDB concentrations are needed for observation.

Particle size and zeta potential of Arg10-PEG-BDB and its DNA complexes were measured 10–15 min after the complex had formed, using dynamic light scattering and electrophoresis method, respectively (ELS-800, Otsuka Electronics Co. Ltd, Osaka, Japan) at 25 °C after the dispersion was diluted to an appropriate volume with water.

2.4. Fluorescence Intensity Distribution Analysis (FIDA)

FIDA was performed with a MF20 microplate reader (Olympus Corp. Tokyo, Japan) using the onboard 543-nm laser at a power of 300 μW for excitation. Experiments were performed in 384-well glass-bottom plates using a sample volume of 50 μL. The FIDA data was analyzed with the MF20 software package. All single-molecule FIDAs were performed under identical conditions with respect to incubation (10 min) at room temperature. The interaction between Arg10-PEG-BDB and DNA experiments were performed using the rhodamine-labeled DNA. The concentration of the labeled DNA was held constant whereas the concentration of Arg10-PEG-BDB was varied in water.

2.5. Phase Contrast Cryo-TEM and Microscopy

Specimens for electron microscopy were prepared on Quantifoil® R1.2/1.3 holed carbon grids at a Leica EM CPC cryo-preparation station. Cryo-electron microscopy was performed on a JEOL JEM-3100FFC TEM equipped with a field emission gun (FEG), helium temperature specimen stage, omega-type energy filter and Gatan Mega-Scan 795 2 K × 2 K CCD camera. For improved contrast of ice-embedded specimens, we employed a novel Zernike-type phase plate at the back focal plane of the objective lens.[18, 19] It provides a true phase contrast regime revealing details in the image that are hidden in the conventional defocus phase contrast mode. All images were taken by the CCD camera with the TEM operated at 300 kV acceleration voltage, zero-loss energy filter mode, ×60,000 indicated magnification and employing the phase plate. At that magnification, the specimen resolution at the CCD is 3.0 Å/pix. To minimize electron beam damage, we employed a minimum dose protocol which irradiates the area of interest only during image exposure. The total dose to the specimen was about 6 $e^-/Å^2$.

Arg10-PEG-BDB/DNA complexes were diluted with serum-free DMEM to 1 mL. Incubation with HeLa cells was conducted for 1 h in the absence of serum, and then the cells were washed 5 times with 1 mL of PBS. Unfixed cells were observed with an ECLIPSE TS100/100-F for Epi-fluorescence Observations (Nicon, Tokyo, Japan). The level of contrast and the brightness of the images were adjusted.

2.6. Flow Cytometry

HeLa cells were kindly provided by Toyobo Co., Ltd. (Osaka, Japan). HeLa cells were grown in DMEM supplemented with 10% FBS at 37 °C in a humidified 5% CO_2 atmosphere.

HeLa cells were grown to just before confluence in a 12-well plate. For cellular uptake, Arg10-PEG-BDB/rhodamine-DNA was diluted with DMEM containing 10% FBS to 1 mL. Incubation with HeLa cells was conducted for 3 h in the presence of serum since the cells could not be detached from the wells after incubation in the absence of serum. For inhibition of uptake, cells were preincubated for 30 min at 37 °C with DMEM containing 10% FBS in the presence of EIPA (50 μM). Subsequent incubation of the Arg10-PEG-BDB-NBD/DNA was carried out for 1 h in the presence of EIPA.

At the end of the incubation, the dishes were washed 3 times with 1 mL of PBS, and the cells were detached with 0.05% trypsin and EDTA solution. The cells were centrifuged at 1500 rpm, and the supernatant was discarded. The cells were resuspended with PBS containing 0.1% BSA and 1 mM EDTA, and directly introduced to a FACSCalibur flow cytometer (Becton Dickinson, San Jose, CA) equipped with a 488 nm argon ion laser. Data for 10000 fluorescent events were obtained by recording forward scatter (FSC) and side scatter (SSC) with green (for NBD; 530/30 nm) and red (for rhodamine; 585/42 nm) fluorescences.

2.7. Gene Transfection

Arg10-PEG-BDB/DNA complexes, prepared by mixing 2 μg of pCMV-luc or pEGFP-C1 with various concentrations of Arg10-PEG-BDB, were diluted with serum-free DMEM to 1 mL.[12] Incubation with HeLa cells was conducted for 3 h in the absence of serum, and cells were cultured for another 21 h in the presence of serum.

Luciferase expression was measured according to the instructions accompanying the luciferase assay system. Incubation was terminated by washing the plates three times with cold phosphate-buffered saline (pH 7.4) (PBS). Cell lysis solution (Pica gene) was added to the cell monolayers and subjected to freezing at −80 °C and thawing at 37 °C, followed by centrifugation at 15000 rpm for 5 s. The supernatants were frozen and stored at −80 °C until the assays. Aliquots of 20 μL of the supernatants were mixed with 100 μL of luciferin solution (Pica gene) and counts per second (cps) were measured with a chemoluminometer (Wallac ARVO SX 1420 multilabel counter, Perkin-Elmer Life Science, Japan, Co. Ltd., Kanagawa, Japan). The protein concentration of the supernatants was determined with BCA reagent using bovine serum albumin as a standard and cps/μg protein was calculated.

GFP expression was analyzed by fluorescence microscopy and flow cytometer. For fluorescence microscopy,

at the end of the incubation, the dishes were washed 3 times with 1 mL of PBS and fixed with 10% formaldehyde PBS at room temperature for 20 min, and washed three times with PBS. Then, the cells were coated with Aqua Poly/Mount (Poly science, Warrington, PA) to prevent fading and covered with coverslips. The fixed cells were observed with an ECLIPSE TS100/100-F for Epi-fluorescence Observations. The contrast level and brightness of the images were adjusted.

2.8. Data Analysis

Significant differences in the mean values were evaluated using Student's unpaired t-test. A p-value of less than 0.05 was considered significant.

3. RESULTS AND DISCUSSION

3.1. Characterization and Transfection Efficiency of Arg10-PEG-BDB

In order to determine the CMC of Arg10-PEG-BDB in water, we monitored fluorescence intensity as we added different concentrations of Arg10-PEG-BDB into an aqueous dispersion of pyrene. The CMC value of Arg10-PEG-BDB was 20.9 μM or 83.6 μg/mL at room temperature (Fig. 2).

Particle size and the zeta-potential of Arg10-PEG-BDB (25 μM)/DNA (N/P = 42.5/1) complex were about 1500 nm and 42.7 mV, respectively (Table I). The zeta-potential of the complex (5 μM, N/P = 8.5/1, 27.1 mV) decreased by about 10 mV compared with that of Arg10-PEG-BDB micelles (38.0 mV) due to the negative charge of DNA.

We examined the influence of the concentration of Arg10-PEG-BDB on transfection efficiency by luciferase activity. The highest transfection efficiency was observed at the concentration of 5 μM of Arg10-PEG-BDB (N/P = 8.5/1), which is significantly (1.5-fold) higher than that of

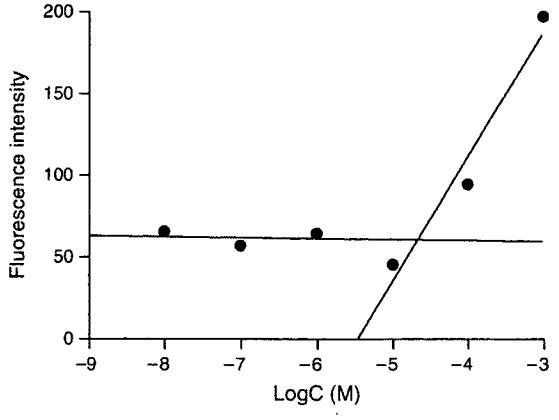

Fig. 2. CMC measurements of Arg10-PEG-BDB by fluorescence probe method using pyrene.

Table I. Particle size and zeta-potential of Arg10-PEG-BDB complexed with or without DNA.

Lipid concentration and complex[a]	N/P	Size (nm)	Zeta-potential (mV)
Arg10-PEG-BDB (25 μM)		N.D.[b]	+38.0
Arg10-PEG-BDB (5 μM)/DNA	8.5/1	N.D.[b]	+27.1
Arg10-PEG-BDB (25 μM)/DNA	42.5/1	~1500	+42.7

[a]Complex with 2 μg of DNA.
[b]N.D., not detected by dynamic light scattering method.

25 μM (Fig. 3(A)), superficially suggesting that micelle formation is not necessary for high transfection efficiency. To examine the distribution of transfection in cells, we observed the transfection efficiency of Arg10-PEG-BDB with the plasmid pEGFP-C1 using flow cytometry and fluorescence microscopy. 5 μM of Arg10-PEG-BDB showed about 7-fold higher transfection efficiencies than 25 μM (Fig. 3(B)). A significantly higher level of GFP protein was observed in the cells treated with 5 μM of Arg10-PEG-BDB than 25 μM, corresponding to the results of luciferase expression (Fig. 3(C)).

The higher concentration of Arg10-PEG-BDB/DNA could not be used because cytotoxicity was increased with an increase of lipid concentration.[12] The cytotoxicity of 5 μM of Arg10-PEG-BDB/DNA, therefore, was lower than that of 25 μM. To clarify the underlying mechanisms that dictated the remarkable differences between 5 and 25 μM in lipid-mediated transfection efficiency, the properties of lipid complexes with DNA were investigated.

3.2. Investigation of the Interaction of Arg10-PEG-BDB with DNA by FIDA

To examine the interaction of Arg10-PEG-BDB with DNA, Arg10-PEG-BDB and 2 μg rhodamine-DNA was mixed and characterized using FIDA with a MF20 microplate reader (Olympus Corp. Tokyo, Japan).[9] A theoretical probability distribution of photon count numbers is fitted against the obtained histogram, yielding specific brightness values Q and concentrations C for all different species in a sample. Decreased C value and increased Q value were observed at the concentration of 1~5 μM of Arg10-PEG-BDB, suggesting that more DNA bound to Arg10-PEG-BDB in this concentration range (Figs. 4(A, B)). The data showed that the interaction of 5 μM of Arg10-PEG-BDB with DNA (N/P = 8.5/1) was stronger than that of 25 μM (N/P = 42.5/1). DNA might help the self-aggregation of Arg10-PEG-BDB even at low concentrations of lipid. This effect may be reflected in the highest transfection efficiency at the 5 μM concentration of Arg10-PEG-BDB to 2 μg DNA. To examine whether this difference of interaction of lipid with DNA in complexes by the concentration of lipid correlated with the differences in structural feature, the complexes were further characterized by electron microscopy.

RESEARCH ARTICLE

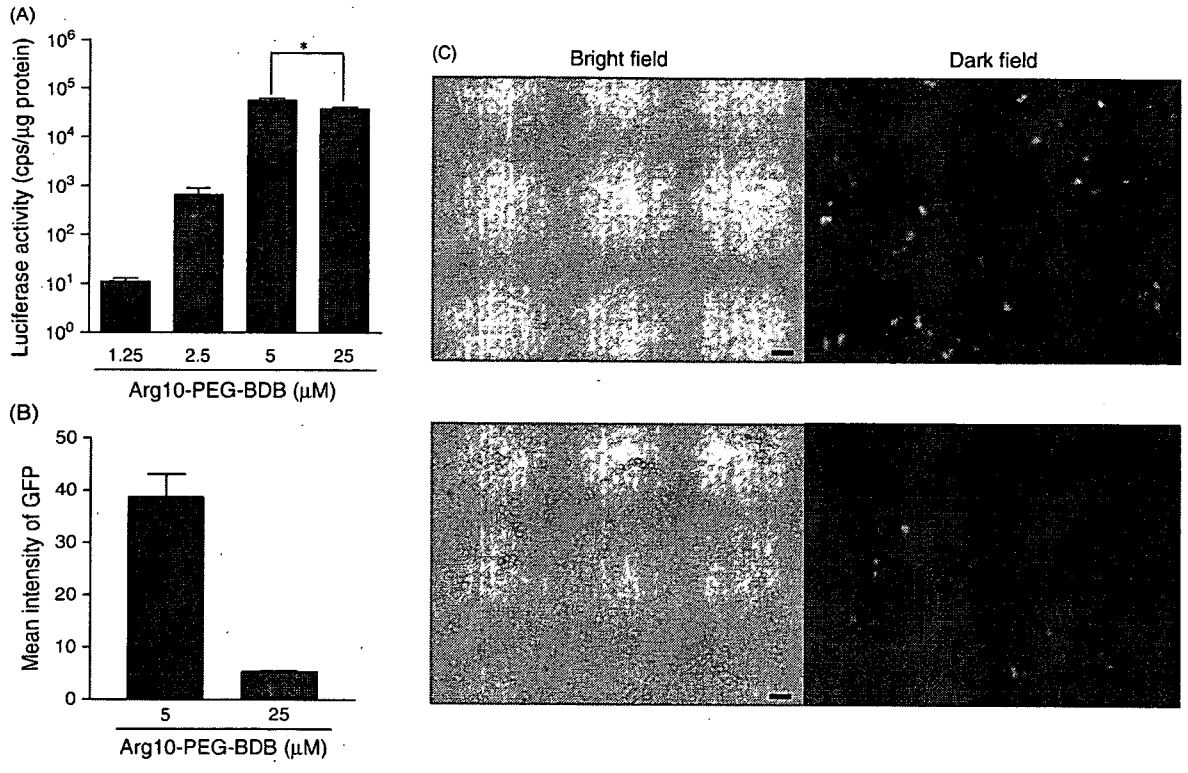

Fig. 3. Influence of the concentration of Arg10-PEG-BDB complexed with DNA on transfection efficiency. Arg10-PEG-BDB/DNA complexes (prepared by mixing 2 μg of pCMV-luc or pEGFP-C1 with various concentrations of Arg10-PEG-BDB) were diluted with serum-free DMEM to a final volume of 1 mL. After incubation for 3 h at 37 °C in serum-free DMEM, DMEM (1 mL) containing 10% FBS was added, and the cells were further incubated for 21 h. (A) Luciferase activity of various concentrations of Arg10-PEG-BDB. (B) GFP expression of 5 or 25 μM of Arg10-PEG-BDB. Each value is the mean ± S.D. of three separate determinations. (C) Analysis of GFP expression by fluorescence microscopy (magnification ×100). 5 μM of Arg10-PEG-BDB (top) and 25 μM of Arg10-PEG-BDB (bottom) are shown. Scale bar = 50 μm.

3.3. The Morphology of Arg10-PEG-BDB/DNA Complexes Determined by Electron Microscopy and Microscopy

To reveal the nanostructure of Arg10-PEG-BDB/DNA complexes under various concentrations of lipid, we observed the Arg10-PEG-BDB/DNA complex using phase contrast cryo-TEM. Free DNA papered was observed as open circular one (data not shown). To observe the lipid structure, two higher concentrations of Arg10-PEG-BDB were examined at the same (N/P) ratio as the transfection experiments. Micellar structures with several nm sizes were observed at 1.25 mM of Arg10-PEG-BDB above CMC (Fig. 5(A)). In Arg10-PEG-BDB/DNA complex (N/P = 8.5/1), a net-like structure was observed in which DNA was involved (Fig. 5(B)). These net-like structures may contribute to high transfection efficiency, but the particle size of Arg10-PEG-BDB (5 μM, 0.25 mM)/DNA (N/P = 8.5/1) in water was not detected by dynamic light scattering method. Surprisingly, in the Arg10-PEG-BDB/DNA complex (N/P = 42.5/1), heterogeneous nanostructures were observed. Other than net-like structures, large fibrous nanostructures were visible (Fig. 5(C)). Their particle size of Arg10-PEG-BDB (1.25 mM)/DNA (N/P = 42.5/1) in water was about 1.5 μm by dynamic light scattering method. In both cases we can clearly see DNA molecules around the edge of the net-like structures.

At a lower magnification, we observed the structure at the same condition as the transfection by the microscopy. Cells were exposed for 1 h to the 5 or 25 μM of Arg10-PEG-BDB/DNA complex in the absence of serum. Next, the unfixed cells were visualized by microscopy. It was hardly observed in 5 μM of Arg10-PEG-BDB/DNA, but a large aggregation was observed in 25 μM (Figs. 6(A, B)). The large aggregation of 25 μM of Arg10-PEG-BDB/DNA, therefore, might inhibit the cell internalization or the release of DNA from endosomes into cytoplasm.

Increase of lipid concentration appeared to tend to convert from net-like structures into a large fibrous one. Previously, we reported that the structure of PEG-BDB became fiber with the increase of lipid concentration.[20] At higher concentration of Arg10-PEG-BDB, DNA might induce the fibrous nanostructure by partial neutralization of Arg10-PEG-BDB, suggesting that DNA may modulate the net-like structure and fibrous nanostructure of Arg10-PEG-BDB. The former reflected a stronger interaction between DNA and lipid than the latter. To further investigate effect of the difference of nanostructures of complexes

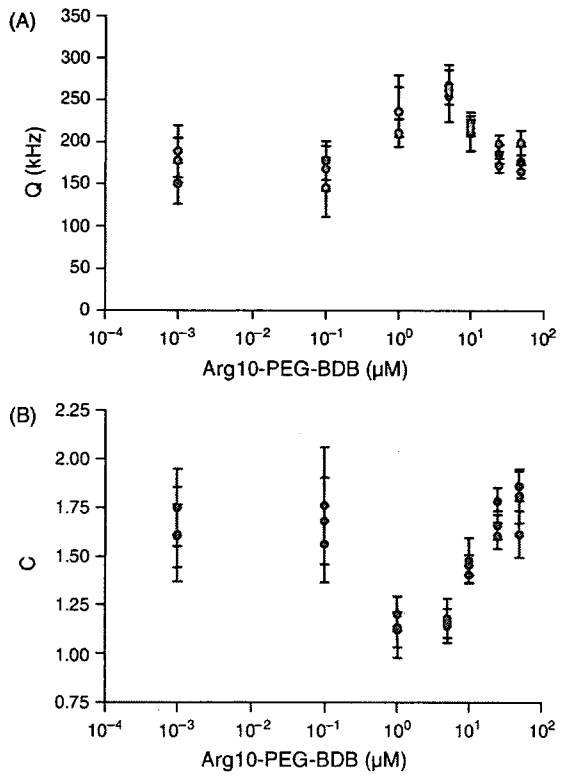

Fig. 4. Fluorescence intensity distribution analysis (FIDA) of Arg10-PEG-BDB and 2 μg rhodamine-DNA complex. (A) Brightness per complex; Q value. (B) Fluorescent DNA number; C value. Each value is the mean ± S.D. of three separate determinations.

on transfection efficiency, cellular uptake mechanism was subsequently examined.

3.4. Cellular Uptake Mechanism

The difference of nanostructures of complexes may cause difference in the ability to deliver DNA into HeLa cells. At first, to examine the association of Arg10-PEG-BDB/DNA complex with cells, we assayed the cell internalization of 5 or 25 μM of the Arg10-PEG-BDB/DNA 3 h after transfection with serum by flow cytometry (Fig. 7(A)). To remove bind Arg10-PEG-BDB/DNA on the surface of plasma membrane, we washed the cells with PBS and treated them with trypsin.[21] Associated amount of 5 or 25 μM of Arg10-PEG-BDB/DNA with the cells was almost same, indicated that both concentrations of Arg10-PEG-BDB were able to carry similar amount of rhodamine-DNA into cells.

The cellular uptake pathway is reported to be different depending on the density of octaarginine (Arg8) in liposome containing Arg8.[22] Hence, there is a possibility that the cellular uptake mechanism might change depending on the concentration of Arg10-PEG-BDB. The translocation of Tat and Arg8 peptide are suggested to occur through macropinocytosis which is dependent on lipidic

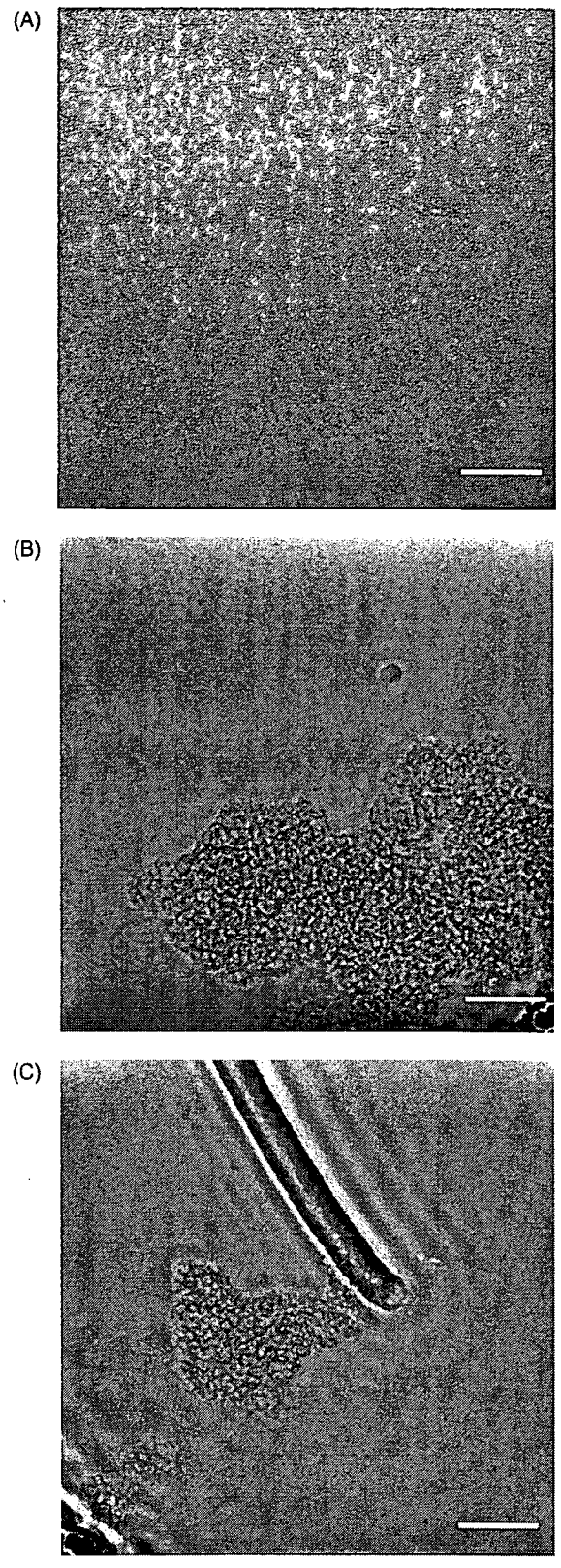

Fig. 5. Phase contrast cryo-TEM analysis of the complex structure of Arg10-PEG-BDB and DNA. (A) 1.25 mM of Arg10-PEG-BDB. (B) 0.25 mM of Arg10-PEG-BDB/DNA (N/P = 8.5/1). (C) 1.25 mM of Arg10-PEG-BDB/DNA (N/P = 42.5/1). Scale bar = 100 nm.

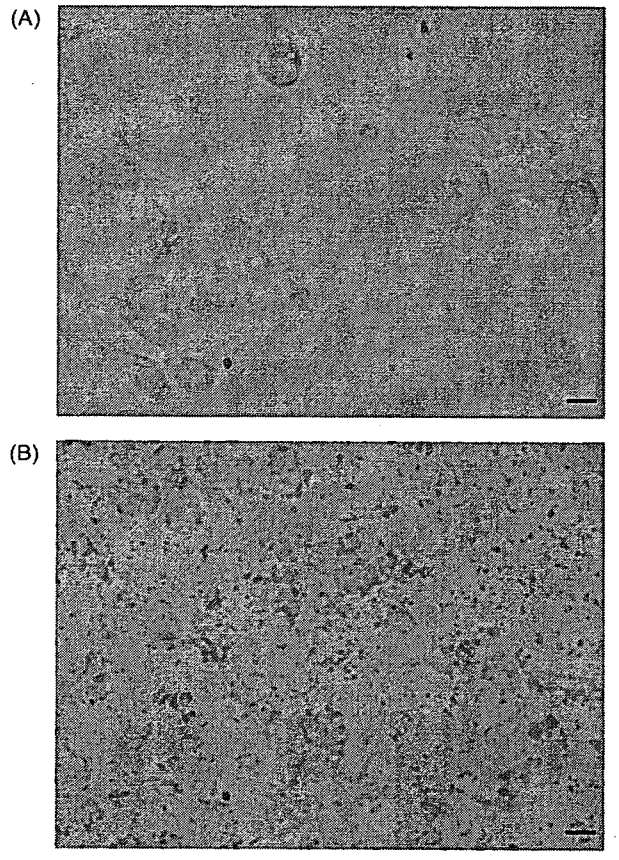

Fig. 6. Microscopic analysis of the Arg10-PEG-BDB/DNA complex incubated with the cells for 1 h at 37 °C in serum-free DMEM. The unfixed cells were observed with a microscope. (A) 5 μM of Arg10-PEG-BDB/DNA (N/P = 8.5/1). (B) 25 μM of Arg10-PEG-BDB/DNA (N/P = 42.5/1). Scale bar = 20 μm.

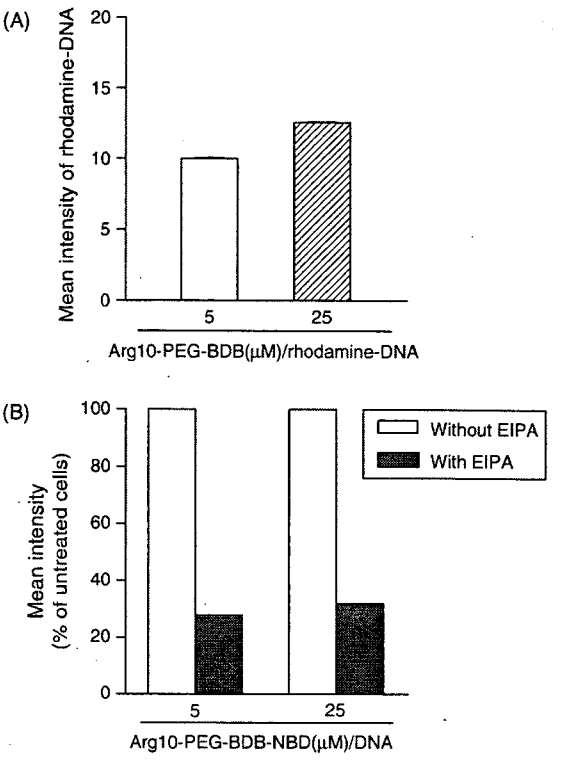

Fig. 7. (A) Cellular uptake of 5 or 25 μM of Arg10-PEG-BDB/rhodamine-DNA incubated for 3 h at 37 °C. The cells were treated with trypsin before flow cytometry. (B) Effect of EIPA on their cellular uptake. Cells were pretreated with EIPA (50 μM) at 37 °C for 30 min. Medium was replaced with fresh medium containing 5 or 25 μM Arg10-PEG-BDB-NBD/2 μg DNA. Cells were incubated for 1 h at 37 °C in serum DMEM containing EIPA (50 μM). Each value is the mean ± S.D. of three separate determinations.

microdomains.[23,24] Macropinocytosis is a kind of endocytosis as a cellular uptake pathway.[25] Macropinosomes are formed by actin-driven ruffling of the plasma membrane, followed by folding and pinching off of irregular-sized vesicles.[26] Macropinocytosis is inhibited by 5-(*N*-ethyl-*N*-isopropyl) amiloride (EIPA), which inhibits Na^+/H^+ exchange protein.[23] To examine the internalization mechanism of 5 and 25 μM Arg10-PEG-BDB/DNA (N/P = 8.5/1 and 42.5/1), we investigated the effect of EIPA on the cellular uptake of complexes, using Arg10-PEG-BDB-NBD (Fig. 7(B)). Arg10-PEG-BDB-NBD (5 and 25 μM)/DNA showed about 70% lower internalization efficiency at 50 μM of EIPA than in its absence. This finding suggests that 5 and 25 μM of Arg10-PEG-BDB/DNA were taken up via a macropinocytosis pathway although their structures were different (Figs. 5(B, C)). DNA may be released easily in the cytoplasm because it is reported that macropinosomes are leaky.[27] The large fibrous nanostructure, therefore, might inhibit the release of DNA from macropinosomes into cytoplasm. At the present research technique, it is difficult to examine it further since the research of CPP should be observed at unfixed cells.

4. CONCLUSIONS

Arg10-PEG-BDB at the concentration below CMC showed higher transfection efficiency in HeLa cells than that above CMC. In Arg10-PEG-BDB/DNA complex below CMC, a net-like structure was observed. On the other hand, in the Arg10-PEG-BDB/DNA complex above CMC, heterogenous structures composed of net-like and large fibrous structures were observed. It is very important that plasmid DNA is able to help Arg10-PEG-BDB to form supramolecular structures. DNA-assisted Arg10-PEG-BDB nanostructure formation may result in concentration-dependent transfection efficiency.

Acknowledgments: This project was supported in part by a grant from the Promotion and Mutual Aid Corporation for Private Schools of Japan and by a Grant-in-Aid for Scientific Research from the Ministry of Education, Culture, Sports, Science, and Technology of Japan. This study was supported in part by the Ministry of Education, Culture, Sports, Science and Technology, Japan, and by the Open Research Center Project.

RESEARCH ARTICLE

References and Notes

1. T. Niidome and L. Huang, *Gene Ther.* 9, 1647 (**2002**).
2. E. Marshall, *Science* 286, 2244 (**1999**).
3. P. L. Felgner, T. R. Gadek, M. Holm, R. Roman, H. W. Chan, M. Wenz, J. P. Northrop, G. M. Ringold, and M. Danielsen, *Proc. Natl. Acad. Sci. U.S.A.* 84, 7413 (**1987**).
4. T. B. Potocky, J. Silvius, A. K. Menon, and S. H. Gellman, *Chembiochem* 8, 917 (**2007**).
5. D. J. Mitchell, D. T. Kim, L. Steinman, C. G. Fathman, and J. B. Rothbard, *J. Pept. Res.* 56, 318 (**2000**).
6. P. A. Wender, D. J. Mitchell, K. Pattabiraman, E. T. Pelkey, L. Steinman, and J. B. Rothbard, *Proc. Natl. Acad. Sci. U.S.A.* 97, 13003 (**2000**).
7. S. Futaki, T. Suzuki, W. Ohashi, T. Yagami, S. Tanaka, K. Ueda, and Y. Sugiura, *J. Biol. Chem.* 276, 5836 (**2001**).
8. S. Futaki, W. Ohashi, T. Suzuki, M. Niwa, S. Tanaka, K. Ueda, H. Harashima, and Y. Sugiura, *Bioconjug. Chem.* 12, 1005 (**2001**).
9. M. Furuhata, H. Kawakami, K. Toma, Y. Hattori, and Y. Maitani, *Bioconjug. Chem.* 17, 935 (**2006**).
10. K. Kogure, R. Moriguchi, K. Sasaki, M. Ueno, S. Futaki, and H. Harashima, *J. Control. Release* 98, 317 (**2004**).
11. W. J. Kim, L. V. Christensen, S. Jo, J. W. Yockman, J. H. Jeong, Y. H. Kim, and S. W. Kim, *Mol. Ther.* 14, 343 (**2006**).
12. M. Furuhata, H. Kawakami, K. Toma, Y. Hattori, and Y. Maitani, *Int. J. Pharm.* 316, 109 (**2006**).
13. M. X. Tang and F. C. Szoka, *Gene Ther.* 4, 823 (**1997**).
14. J. Smisterova, A. Wagenaar, M. C. A. Stuart, E. Polushkin, G. ten Brinke, R. Hulst, J. B. F. N. Engberts, and D. Hoekstra, *J. Biol. Chem.* 276, 47615 (**2001**).
15. B. Pitard, O. Aguerre, M. Airiau, A. M. Lachages, T. Boukhnikachvili, G. Byk, C. Dubertret, C. Herviou, D. Scherman, J. F. Mayaux, and J. Crouzet, *Proc. Natl. Acad. Sci. U.S.A.* 94, 14412 (**1997**).
16. S. Igarashi, Y. Hattori, and Y. Maitani, *J. Control. Release* 112, 362 (**2006**).
17. C. L. Zhao, M. A. Winnik, G. Riess, and M. D. Croucher, *Langmuir* 6, 514 (**1990**).
18. R. Danev and K. Nagayama, *Ultramicroscopy* 88, 243 (**2001**).
19. K. Nagayama, *Adv. Imag. Elect. Phys.* 138, 69 (**2005**).
20. T. Yoshitomi, S. Yabuki, H. Kawakami, R. Sato, K. Toma, M. Furuhata, and Y. Maitani, *Colloids. Surf. A Physicochem. Eng. Asp.* 284–285, 276 (**2006**).
21. J. P. Richard, K. Melikov, E. Vives, C. Ramos, B. Verbeure, M. J. Gait, L. V. Chernomordik, and B. Lebleu, *J. Biol. Chem.* 278, 585 (**2003**).
22. I. Khalil, K. Kogure, S. Futaki, and H. Harashima, *J. Biol. Chem.* 281, 3544 (**2006**).
23. J. S. Wadia, R. V. Stan, and S. F. Dowdy, *Nat. Med.* 10, 310 (**2004**).
24. I. Nakase, M. Niwa, T. Takeuchi, K. Sonomura, N. Kawabata, Y. Koike, M. Takehashi, S. Tanaka, K. Ueda, J. C. Simpson, A. T. Jones, Y. Sugiura, and S. Futaki, *Mol. Ther.* 10, 1011 (**2004**).
25. S. D. Conner and S. L. Schmid, *Nature* 422, 37 (**2003**).
26. S. Grimmer, B. van Deurs, and K. Sandvig, *J. Cell Sci.* 115, 2953 (**2002**).
27. O. Meier, K. Boucke, S. V. Hammer, S. Keller, R. P. Stidwill, S. Hemmi, and U. F. Greber, *J. Cell Biol.* 158, 1119 (**2002**).

Received: 3 October 2007. Accepted: 23 October 2007.

RESEARCH ARTICLE

Int. J. Cancer: **122**, 689–698 (2008)

p-Dodecylaminophenol derived from the synthetic retinoid, fenretinide: Antitumor efficacy *in vitro* and *in vivo* against human prostate cancer and mechanism of action

Noriko Takahashi*, Yusuke Watanabe, Yoshie Maitani, Takayasu Yamauchi, Kimio Higashiyama and Toshihiro Ohba

Laboratory of Physiological Chemistry, Institute of Medicinal Chemistry, Hoshi University, Shinagawa, Tokyo 142-8501, Japan

Fenretinide, *N*-(4-hydroxyphenyl)retinamide (4-HPR) is an aminophenol-containing synthetic retinoid derivative of all-*trans*-retinoic acid, which is a potent chemopreventive and antiproliferative agent against various cancers. Clinical studies of 4-HPR have shown side effects consisting of night blindness and ocular toxicity. To maintain potent anticancer activity without side effects, *p*-dodecylaminophenol (*p*-DDAP) was designed based on structure–activity relationships of 4-HPR. In our study, we investigate whether *p*-DDAP shows anticancer activity against human prostate cancer cell line PC-3 when compared with 4-HPR. *p*-DDAP inhibited PC-3 cell growth progressively from low to high concentration in a dose-dependent manner. *p*-DDAP was the most potent antiproliferative agent *in vitro* among 6 *p*-alkylaminophenols and 3 4-hydroxyphenyl analogs examined including 4-HPR. Cells treated with *p*-DDAP were shown to undergo apoptosis, based on condensation nuclei, cytofluorimetric analysis, propidium iodide staining and the expression of *bcl-2* and caspase 3. *p*-DDAP arrested the S phase of the cell cycle, while 4-HPR arrested the G_0/G_1 phase. In addition, both the i.v. and i.p. administration of *p*-DDAP suppressed tumor growth in PC-3-implanted mice *in vivo*. *p*-DDAP showed no effects on blood retinol concentrations, in contrast to reductions after 4-HPR administration. These results indicate that *p*-DDAP exhibits excellent anticancer efficacy against hormonal independent prostate cancer *in vitro* and *in vivo*, and it may have great potential for clinical use in the treatment of prostate cancer with reduced side effects.

Key words: aminophenol; anticancer; retinoid; prostate cancer; apoptosis

N-(4-Hydroxyphenyl)retinamide (4-HPR, fenretinide) (Fig. 1, middle), a synthetic amide of all-*trans*-retinoic acid (RA), is an effective anticancer drug,[1–5] which is used against a wide variety of tumor types. 4-HPR currently is in clinical trials for the treatment of breast, bladder, renal and neuroblastoma malignancies.[6–11] However, studies have shown that treatment of patients with 4-HPR is accompanied by night blindness because of a decrease in serum retinol levels.[12] It appears that this side effect occurs by the displacement of retinol from serum retinol binding protein (RBP), resulting in reduced delivery of retinol to eye.[13–15]

The mechanisms behind the anticancer effects of 4-HPR are unclear. It is generally accepted that 4-HPR may act *via* pathways which are independent of the nuclear retinoid receptors, RARs and RXRs, since 4-HPR exhibits extremely poor binding to nuclear retinoid receptors, and it shows anticancer activity against cells resistant to RA. Therefore, 4-HPR may act on cells directly rather than through hydrolysis to free RA. On the basis of structure–activity relationships of 4-HPR, we recently designed *p*-alkylaminophenols without aromatic rings that have markedly different structures from retinol, RA and 4-HPR. We showed that the *p*-methylaminophenol moiety in 4-HPR contributes most significantly to its anticancer activity when compared with the 4-aminophenol and *p*-aminoacetophen moieties.[16,17] The elongation of the polymethylene chain in *p*-methylaminophenol increases the anticancer activity, and *p*-octylaminophenol (*p*-OAP) among *p*-aminophenols with various lengths of alkyl chains (C_1–C_8) examined was the most potent inhibitor of cell growth against various cancer cell lines, including human leukemia cell lines, HL60 and HL60R, which are resistant to RA.[18] Furthermore, we synthesized novel aminophenol analogs (C_{10}–C_{12}) that bear carbon side-chain lengths similar to those of 4-HPR (Fig. 1, middle), and we examined the antioxidant and antiproliferative properties of these analogs.[19,20] We found that *p*-dodecylaminophenol (*p*-DDAP, Fig. 1, top) and *p*-decylaminophenol (*p*-DAP) exhibited both activities greater than 4-HPR did.

Prostate cancer is a chronic disease in men. Despite advances in the understanding of prostate cancer cell biology, the lack of early detection and the development of androgen independence during commonly used anti-androgen therapies of prostate cancer are problematic. At present, there is no cure for advanced prostate cancer once it has progressed to an androgen-independent stage. Hormonal therapy, radiotherapy and chemotherapy are of limited efficacy for prostate cancer patients diagnosed with androgen-independent disease. Therefore, the development of chemopreventive agents against hormonal independent prostate cancer is of critical importance.

Thus, we set out to examine whether *p*-DDAP is effective against the hormonal independent human prostate cancer cell line PC-3 *in vitro*, what is the mechanism of anticancer activity by *p*-DDAP and whether *p*-DDAP is efficacious against prostate cancer *in vivo* without side effects. The results of these studies are presented herein.

Material and methods

Chemicals

RA, ethylenediaminetetraacetic acid (EDTA), bovine serum albumin (BSA, fraction V) and dimethylsulfoxide (DMSO) were obtained from Sigma Chemical (St. Louis, MO). 4-HPR was provided by Dr. R. C. Moon, University of Illinois, Chicago, IL. *p*-Methylaminophenol (*p*-MAP) was purchased from Nacalai Tesque. (Kyoto, Japan). All other chemicals were of reagent grade. *N*-(4-Hydroxyphenyl)dodecananamide (4-HPDD), *N*-(4-hydroxyphenyl)decananamide (4-HPD), *p*-DDAP, *p*-DAP, *p*-OAP, *p*-hexylaminophenol (*p*-HAP) and *p*-butylaminophenol (*p*-BAP) were synthesized as described previously.[18,19,21]

Abbreviations: EDTA, ethylenediaminetetraacetic acid; MTT, 3-(4,5-dimethylthiazol-2-yl)-2,5-diphenyltetrazolium bromide; PBS, phosphate-buffered saline (1.5 mM KH_2PO_4, 8.1 mM Na_2HPO_4, 136.9 mM NaCl, pH 7.2); *p*-DAP, *p*-decylaminophenol, 4-(decylamino)phenol; *p*-DDAP, *p*-dodecylaminophenol, 4-(dodecylamino)phenol; RA, retinoic acid; RAR, retinoic acid nuclear receptor; RBP, retinol binding protein; RT-PCR, reverse transcription-polymerase chain reaction; 4-HBR, 4-hydroxybenzylretinone; 4-HPD, *N*-(4-hydroxyphenyl)decananamide, *p*-decanoylaminophenol; 4-HPDD, *N*-(4-hydroxyphenyl)dodecananamide, *p*-dodecanoylaminophenol; 4-HPR, *N*-(4-hydroxyphenyl)retinamide, fenretinide.

Grant sponsor: The Ministry of Education, Culture, Sports, Science and Technology, Japan and the Open Research Center Project.

***Correspondence to:** Laboratory of Physiological Chemistry, Institute of Medicinal Chemistry, Hoshi University, 2-4-41, Ebara, Shinagawa, Tokyo 142-8501, Japan. Fax: +81-3-5498-5950.
E-mail: t-noriko@hoshi.ac.jp

Received 7 August 2007; Accepted after revision 22 August 2007
DOI 10.1002/ijc.23154
Published online 22 October 2007 in Wiley InterScience (www.interscience.wiley.com).

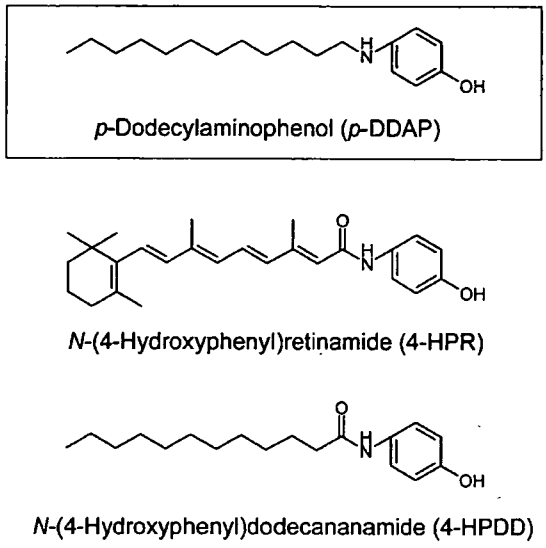

FIGURE 1 – Chemical structures of *p*-DDAP, 4-HPR and 4-HPDD.

Cell

Early passage (<30) human myeloid leukemia cell lines, HL60 and HL60R, a mutant subclone of HL60 that exhibited relative resistance to RA and that harbors RARs with markedly reduced affinity for RA, were maintained in RPMI 1640 medium (GIBCO, Grand Island, NY) supplemented with 10 mM 4-(2-hydroxyethyl)-1-piperazinethanesulfonic acid (HEPES), pH 7.3 and 10% fetal bovine serum (FBS; GIBCO).[22,23]

Human breast cancer cell lines, MCF-7 and MCF-7/Adr^R were obtained from the American Type Culture Collection (ATCC), Rockville, MD.[24] Cells were maintained in Iscove's Modified Dulbecco's Medium supplemented with 10% heat-inactivated FBS (GIBCO). Human hepatoma cell line HepG2[25] was obtained from RIKEN cell bank (Tokyo, Japan). Human prostate cancer cell line DU-145[26] was obtained from Dr. Y. Pommier of the National Cancer Institute (Bethesda, MD). HepG2 and DU-145 cells were grown in RPMI medium containing 10% FBS.

Another human prostate cancer cell line PC-3 was obtained from ATCC. PC 3 cells were grown in RPMI medium containing 10% FBS and penicillin/streptomycin (50 units/ml, 50 μg/ml). Attached cells were removed from the tissue-culture flask surface with trypsin-EDTA (GIBCO).

All cells described above were incubated at 37°C in a humidified atmosphere of 5% CO_2 in air.

Cell growth

HL60 and HL60R cells (1×10^5 cells/ml) were grown in RPMI 1640 medium containing 10% FBS with 4 μM *p*-DDAP and 4-HPR for 94 and 65 hr, respectively. Cell number was estimated by an electric particle counter (Coulter Electronics, Hialeah, FL) and viability by trypan blue dye exclusion. The percentage of net growth is shown with values adjusted by subtracting the initial cell concentration of experimental cultures from the initial concentration of control cultures which were defined as 100%. Values for percent net cell growth were calculated with the following formula: [(cell concentration of experimental culture) − (initial cell concentration)/(cell concentration of control culture) − (initial cell concentration)] × 100.

MCF-7, MCF-7/Adr^R, HepG2 and DU-145 cells were trypsinized and suspended in RPMI 1640 medium containing 10% FBS. Cells (0.5×10^4 cells/ml) were incubated at 37°C in a humidified atmosphere of 5% CO_2 in air. After 1 day, 4 μM *p*-DDAP and 4-HPR were added to the cultures. Cells were incubated for 68 hr, and then viable cell number was estimated using 3-(4,5-dimethylthiazol-2-yl)-2,5-diphenyltetrazolium bromide (MTT) as described previously.[27] PC-3 cells were trypsinized and suspended in RPMI 1640 medium containing 10% FBS and penicillin/streptomycin (50 units/ml, 50 μg/ml). Cells (5×10^4 cells/ml) were incubated at 37°C in a humidified atmosphere of 5% CO_2 in air. After 1 day, various concentrations of *p*-DDAP, *p*-DAP, *p*-OAP, *p*-HAP, *p*-BAP, *p*-MAP, 4-HPDD, 4-HPD and 4-HPR were added to the cultures. Cells were incubated for 48–54 hr, and then viable cell number was estimated using MTT as described previously.[27] Values for percent net cell growth were calculated with the following formula: [(absorbance of experimental cell concentration) − (absorbance of initial cell concentration)/(absorbance of control cell concentration) − (absorbance of initial cell concentration)] × 100.

Morphologic evaluation of apoptosis

Exponentially growing PC-3 cells (5×10^4 cells/ml) were seeded in a chamber slide (NUNC, Roskilde, Denmark) and incubated at 37°C in a humidified atmosphere of 5% CO_2 in air. After 1 day, 4 μM *p*-DDAP, 4-HPDD, and 4-HPR were added to cell cultures. Cells were incubated for 17 hr, and then fixed and stained with Wright-Giemsa staining solution. Morphological changes were visualized by light microscopy.

Measurement of apoptosis

Apoptosis analyses were performed using the Annexin V-FITC Apoptosis Detection Kit (Calbiochem, Catalog No. PF032-1EA, San Diego, CA) following the manufacturer's instructions. Apoptosis and cell viability were measured by staining using annexin V-FITC and propidium iodide (PI), and the stained cells were analyzed immediately by fluorescence activated cell sorting (FACS) calibur flow cytometry (Becton Dickinson, San Jose, CA).

Cell cycle analysis

Cell cycle distribution was determined by flow cytometry after staining the cells with PI. Briefly, PC-3 cells (5×10^4 cells/ml) treated with various concentrations of compounds were harvested and then washed with FACS Buffer (0.1% BSA and 1 mM EDTA in PBS). Cells (1×10^6 cells, 0.5 ml) were fixed in 70% ethanol at 4°C overnight. Before the analysis, cells were centrifuged (750 *g*, 10 min) and washed twice with FACS Buffer to remove ethanol. Cells were then treated with RNaseA (50 ng/ml, 500 μl) at room temperature for 30 min. After the addition of PI (500 μg/ml, 25 μl), cells were incubated for 5 min at room temperature in the dark. The stained cells were analyzed by FACS calibur flow cytometer (Becton Dickinson), equipped with a 488-nm argon ion laser. Data for 10,000 fluorescent events were obtained by recording forward scatter (530 ± 15 nm) and side scatter (~650 nm) fluorescence.

Caspase 3 assay

PC-3 cells treated with various compounds were lysed in lysis buffer [50 mM Tris-HCl (pH 7.4), 1% NP-40, 0.25% sodium deoxycholate, 150 mM NaCl, 1 mM EDTA, 1 mM phenylmethylsulfonyl fluoride, 1 mM sodium fluoride and protease inhibitor cocktail (Calbiochem)]. Cell suspensions were incubated at 4°C for 30 min, and centrifuged at 6,000*g* for 20 min at 4°C. The supernatants (20 μg) were separated by 15% SDS-polyacrylamide gel electrophoresis and immunoreactivity with anti-caspase 3 (Upstate, Lake Placid, NY) was demonstrated by ECL plus Western Blotting System (Amersham Biosciences, UK). Caspase 3 activities were measured by Caspase-3/CPP32 Colorimetric Assay Kit according to manufacturer's instructions (MBL, Nagoya, Japan).

RT-PCR

Total RNA was prepared from PC-3 cells treated with various compounds using Rneasy Plant Mini Kit (Qiagen, MD) according

to the manufacturer's instructions. For RT analysis, 5 μg of RNA were reverse-transcribed using the Moloney murine leukemia virus reverse transcriptase, human placenta RNase inhibitor and random hexadeoxynucleotide primer. The RT reactions were then amplified with specific primers for *bcl-2* (sense: TGCACC-TGACGCCCTTCAC, antisense: AGACAGCCAGGAGAAATC-AAA CAG, 293 bp) and β-actin by PCR. The PCR products were separated by electrophoresis in 3% agarose gel and visualized.

Preparation of microemulsions

Microemulsions were composed of polyethylene glycol 2000-distearoylphosphatidyl-ethanolamine/cholesterol/vitamin E/*p*-DDAP (3:3:3:0.518, weight ratio; 6.3:43.8:39.3:10.6, molar ratio). Microemulsions were prepared by a modified ethanol injection method as described previously.[28,29] The *p*-DDAP-loading efficiency was determined by Sephadex G-50 chromatography and a fluorescence detector[28,29] and also confirmed by measuring the *p*-DDAP amount of the microemulsion fraction using high-pressure liquid chromatography (HPLC) as described below.

Quantitation of p-DDAP and 4-HPR

p-DDAP and 4-HPR entrapped in microemulsions were extracted with equivalent volumes of ethyl acetate containing 1% acetic acid. Compounds in organic layers were analyzed by HPLC using a Shimadzu LC-6A high-pressure pump, Shimadzu CTO-10AS column oven including injector and a SPD-6A UV spectrophotometric detector (Shimadzu, Kyoto, Japan). A LUNA column (5μ C_{18} (2), 150 mm × 4.6 mm, Phenomenex, Rancho Palos Verdes, CA) was used to separate *p*-DDAP, other *p*-alkylaminophenols and 4-HPR. The column was eluted with 80% MeOH, 20% H_2O and 10 mM ammonium acetate at a flow rate of 1.0 ml/min. *p*-DDAP and 4-HPR were detected with UV monitoring at 240 and 350 nm, respectively. Elution time was 17.5 min for *p*-DDAP or 23 min for 4-HPR.

Animals and inoculation of tumor xenografts

Specific pathogen-free athymic BALB/c *nu/nu* nude mice (6 weeks of age, male) were purchased from CLEA Japan (Tokyo, Japan). To generate tumor xenografts, mice were injected subcutaneously (s.c.) in the flank with PC-3 cells (1×10^6 cells) in 0.1 ml of the medium containing 50% Matrigel. When tumors had grown to an average volume of 50–100 mm^3, mice were divided into 3 experimental groups ($n = 6$), which received the following treatments by i.p. injection with vehicle, *p*-DDAP (15 mg/kg) and 4-HPR (15 mg/kg) in sterile 0.9% NaCl solution containing 5% ethanol and 1.65 mg/ml BSA as described previously.[30] The administration was done everyday for 2 weeks. Tumor size was measured with calipers every 2 or 3 days, and tumor volume was calculated by the following equation: volume = $1/2 \times (\text{width})^2 \times$ length.

To evaluate antitumor effects of microemulsion containing *p*-DDAP by i.v. administration, mice inoculated s.c. in the flank with PC-3 cells were grouped at random ($n = 6$) (Day 0).[28,29] When tumors had grown to an average volume of 50–100 mm^3, microemulsion containing *p*-DDAP (10 mg/kg) and empty microemulsion as a control were administered by i.v. injection *via* the lateral tail vein every day for 5 days as described previously.[29] On the other hand, *p*-DDAP (40 mg/kg) and vehicle were given to mice by a single i.p. injection. Tumor volume was calculated as described above.

The animal experiments were done under ethical approval from our Institutional Animal Care and Use Committee.

Measurement of plasma retinol concentration

Plasma retinol concentration was measured according to the modified method of Alshafie et al.[31] Sprague-Dawley rats (5 weeks, male, 150–170 g) were treated by i.p. injection with *p*-DDAP (12.5 mg/kg) and 4-HPR (12.5 mg/kg) every day for 7 days ($n = 3$–6).[30] Blood was drawn after final injection and was centrifuged (1,500*g*, 15 min). The supernatants (serum, 500 μl) were extracted with ethyl acetate (500 μl) by mixing for 1 min and were centrifuged (6,000*g*, 5 min) 3 times. The extracts in ethyl acetate were evaporated by speed vac, and the residues were dissolved in methanol (100 μl). The extract (20 μl) was separated by HPLC as described above. The column was eluted with 85% MeOH, 15% H_2O and 10 mM ammonium acetate at a flow rate of 1.0 ml/min for retinol analysis in convenience. Retinoids were detected at 350 nm. Retention time was 15 min for retinol or 12 min for 4-HPR. Measurements were made using the ratio of peak areas to authentic retinol.

TABLE I - GROWTH INHIBITION OF VARIOUS CANCER CELL LINES BY *P*-DDAP AND 4-HPR

Cell lines	Cell growth inhibition (%)	
	p-DDAP	4-HPR
HL6O	75 ± 0.69	58 ± 0.14
HL6OR	89 ± 0.33	83 ± 1.20
MCF-7	66 ± 0.14	62 ± 0.06
MCF-7/Adr^R	99 ± 0.10	60 ± 0.16
HepG2	13 ± 0.45	27 ± 0.44
DU-145	83 ± 0.09	41 ± 0.24

Various cancer cells were grown in the presence of 4 μM *p*-DDAP and 4-HPR in a medium containing 10% FBS. Cell growth inhibition values (%) were calculated according to the following formula: 100 – percent net cell growth.

Statistical analysis and presentation of results

The statistical significance of the data was evaluated by the Student's *t* test. $p < 0.05$, $p < 0.01$ and $p < 0.001$ were considered significant. Each experiment was performed at least 4 times, and most experiments were repeated at least 3 times with consistent results.

Results

Effects on growth of various cancer cell lines by p-DDAP and 4-HPR

Various cancer cell lines (HL60, HL60R, MCF-7, MCF-7/Adr^R, HepG2 and DU-145 cells) were grown in a medium containing 10% FBS in the presence of 4 μM *p*-DDAP (Fig. 1, top). 4-HPR (Fig. 1, middle) at a concentration of 4 μM was used as an internal standard for measuring inhibition of cell growth. Table I shows the percent of cell growth inhibition by *p*-DDAP and 4-HPR. Cell growth inhibition in the presence of *p*-DDAP was ~75% for HL60, 89% for HL60R, 66% for MCF-7, 99% for MCF-7/Adr^R, 13% for HepG2, and 83% for DU-145. In contrast, 4-HPR inhibited cell growth ~58% for HL60, 83% for HL60R, 62% for MCF-7, 60% for MCF-7/Adr^R, 27% for HepG2 and 41% for DU-145. These results indicate that the growth of various cancer cell lines, except HepG2, was suppressed by *p*-DDAP to a greater extent than by 4-HPR, and that *p*-DDAP was a potent inhibitor of DU-145 cells and HL60R and MCF-7/Adr^R cells, which are resistant clones against RA.

Inhibition of PC-3 cell growth by p-DDAP and its analogs

Since the growth of the hormone-refractory human prostate cancer cell line DU-145 was inhibited markedly by *p*-DDAP, we investigated whether *p*-DDAP affects the growth of another hormone-independent human prostate cancer cell line PC-3 when compared with its analogs. 4-HPR was used as an internal standard for measuring inhibition of cell growth.

Initially, we examined effects on PC-3 cell growth of *p*-alkylaminophenols having a variety of lengths of alkyl chains (C_1–C_{12}). As shown in Figure 2*a*, various concentrations of *p*-alkylaminophenols suppressed PC-3 cell growth in dose-dependent fashions (Fig. 2*a*-a).